*applied sciences*

MDPI

*Article*

# Reliability Analysis of Gyrocompass Systems in Offshore Supply Vessels Under Hydro-Meteorological Disturbances and Its Implications for Oil Spill Risk

**Ewa Dąbrowska**

Faculty of Computer Science, Gdynia Maritime University, Morska 81-87, 81-225 Gdynia, Poland; e.dabrowska@wi.umg.edu.pl

## Featured Application

The proposed reliability and probabilistic risk assessment framework can be applied to offshore supply vessels equipped with redundant gyrocompass systems and Dynamic Positioning (DP) systems. The framework supports the identification of hydro-meteorological conditions associated with increased gyrocompass alarm frequency, evaluation of the reliability benefits of redundant navigation sensors, and estimation of the potential contribution of navigation-system failures to oil spill risk. The approach can assist ship operators and safety engineers in reliability assessment, preventive maintenance planning, and risk-informed decision-making for offshore vessel operations.

## Abstract

This study presents a methodology for assessing the reliability of navigation systems in offshore operations, accounting for hydro-meteorological variability and its implications for environmental risk. A semi-Markov model is developed to characterise transitions between hydro-meteorological states. The approach is applied to a gyrocompass system installed aboard an offshore supply vessel operating in the North Sea under varying wind and wave conditions. The system consists of three redundant gyrocompasses, with alarms triggered by deviations exceeding 2° from the median value. Data collected over an 18-month period are used to estimate the durations of individual hydro-meteorological states and the associated state-transition characteristics, which are subsequently incorporated into the reliability analysis. The resulting alarm-related reliability estimates are then integrated into a probabilistic framework linking deviations in gyrocompass readings to potential loss of navigation performance, accident occurrence and oil spill risk. These estimates are based on operational heading-deviation alarm data, while the conditional risk probabilities are calculated using literature-informed parameters and values adopted for the illustrative risk scenario. Under the assumption of independent gyrocompass events, the three-gyrocompass configuration improves the modelled system reliability and yields a relative reduction of approximately 76.66% in the estimated oil spill probability for the considered time horizon, compared with a single-gyrocompass configuration. This reduction is specific to the adopted risk scenario. The framework therefore provides a basis for risk-informed decision-making in offshore vessel operations.

**Keywords:** navigation system reliability; stochastic modelling; probabilistic risk modelling; hydro-meteorological conditions; gyrocompass; offshore supply vessel; oil spill risk

Check for updates

Academic Editor: José A. Orosa García

Received: 23 September 2026
Revised: 21 October 2026
Accepted: 21 October 2026
Published: 26 October 2026

**Copyright:** © 2026 by the author. Licensee MDPI, Basel, Switzerland. This article is an open access article distributed under the terms and conditions of the Creative Commons Attribution (CC BY) license.

## 1. Introduction

Reliable navigation systems are essential to the safety of offshore maritime operations [1–3]. These activities involve specialised vessels performing complex logistical and operational tasks under challenging environmental conditions. Among these vessels, Platform Supply Vessels (PSVs) operate in close proximity to offshore infrastructure, transporting equipment, drilling materials, and other supplies between offshore installations and coastal bases. Such activities require precise positioning and heading control [4,5].

Modern offshore vessels, including PSVs, anchor-handling tug supply (AHTS) vessels and drill ships, are typically equipped with Dynamic Positioning (DP) systems that use multiple sensor inputs to maintain position and heading despite environmental disturbances such as wind, waves or currents [6,7]. Loss or degradation of heading information may impair DP control, potentially leading to loss of station-keeping. In offshore environments, this may result in collisions or other operational incidents [7,8]. Such incidents may also result in pollution, particularly during cargo transfer or operations conducted near hydrocarbon installations [9,10]. Although navigation system failures are rarely the sole cause of such events, they can act as initiating or contributing factors within complex accident sequences [11–14]. Nevertheless, the mechanism by which sensor-level degradation propagates through DP control loops towards system-level failures remains insufficiently formalised.

Despite the recognised importance of navigation system reliability, its direct linkage to environmental risk has not been sufficiently quantified. Existing studies typically address system reliability [15–19], accident consequences [20] or DP-related loss of position events [21,22] separately, without explicitly modelling the propagation of sensor-level degradation towards high-impact environmental outcomes such as oil spills. This gap limits the ability to assess how disturbances affecting navigation performance may contribute to broader operational risks and ecological consequences.

The main contribution of this study is the integration of semi-Markov modelling of environmental variability, empirical alarm-based reliability analysis of navigation sensors using operational data from an offshore supply vessel, and consequence-based risk assessment (Figure 1). A sensitivity analysis was also conducted to assess the influence of the adopted risk model parameters on the estimated oil spill probabilities.

The paper is organised as follows. Section 2 presents the background and research context, including maritime risk, navigation system reliability and environmental impact assessment. Section 3 describes the Dynamic Positioning system and gyrocompass operation, with particular emphasis on measurement deviations. Section 4 introduces the methodological framework, including semi-Markov modelling of hydro-meteorological variability, reliability assessment and consequence risk modelling. Section 5 presents the case study of the offshore supply vessel *Troms Capella*, including the analysis of hydro-meteorological observations from the vessel's deck logs, gyrocompass reliability assessment based on heading-deviation alarm records, probabilistic oil spill risk estimation and sensitivity analysis. Section 6 discusses the results, their limitations and their implications for offshore operational safety and environmental risk. Finally, Section 7 presents the conclusions.

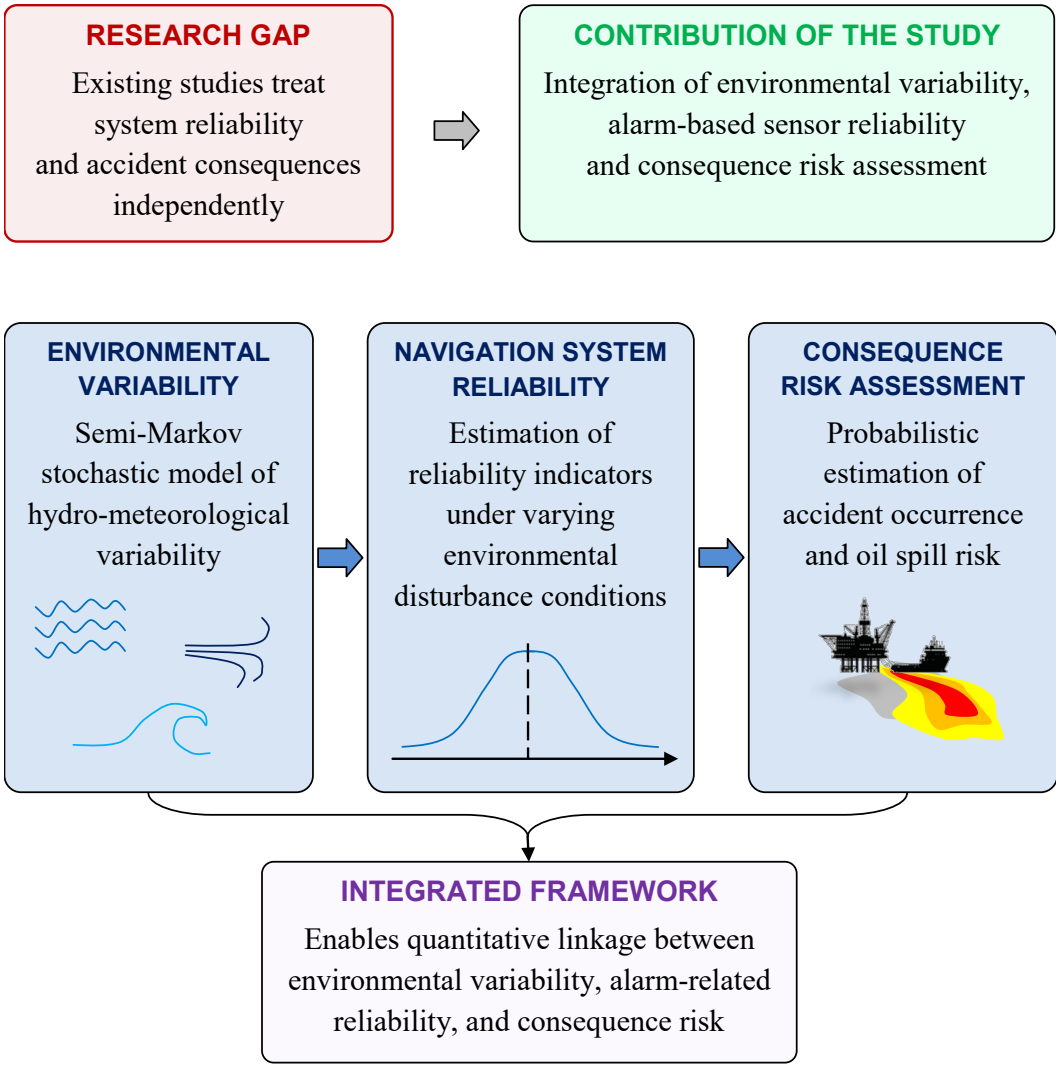



**Figure 1.** Integrated framework for linking environmental variability, navigation system reliability, and consequence risk assessment.

## 2. Background and Research Context

Modern offshore operations rely heavily on dynamically positioned vessels, for which maintaining both position and heading is critical for operational safety and mission success. Dynamic Positioning systems integrate multiple sensor inputs, including position reference systems, motion sensors, wind sensors, and heading reference systems such as gyrocompasses, into a control algorithm that continuously estimates vessel state and compensates for environmental disturbances. Among these components, gyrocompasses play a critical role by providing heading information required for vessel control and position keeping.

Operational reports from offshore industry databases demonstrate that failures of gyrocompass systems can directly contribute to loss of DP capability. For instance, an incident involving the loss of gyrocompass inputs resulted in an uncontrolled vessel excursion of 150 m, requiring emergency recovery procedures [21]. Another documented case involved an incorrect gyro heading that propagated through the DP control model, leading to loss of vessel position during offshore loading operations [23]. Additional accident investigations report that gyrocompass misalignment following power disturbances has resulted in significant navigational deviations and grounding events [24,25]. In one reported case, the gyrocompass was not cross-checked against the magnetic compass following power interruptions [24]. These examples indicate that gyrocompass malfunctions are not merely

isolated sensor issues but can pose system-level safety risks. Studies and offshore incident reports indicate that failures in positioning or navigation systems may contribute to hazardous operational situations [15,21–23]. Under certain conditions, such incidents may lead to oil spills, particularly during drilling, loading, or transfer operations [9,10,20].

The reliability of DP systems and their components has been extensively studied in the context of safety-critical offshore operations, particularly in relation to drilling and subsea intervention, using approaches such as Markov models, failure mode and effects analysis (FMEA) and fault-tree analysis [15,17–19]. Recent studies have analysed the reliability of DP control systems using FMEA and Markov models [18] and reviewed methods applied to DP reliability assessment, including fault trees, Markov models and Bayesian networks [19]. Other research has addressed compass indication integrity using heading-error analysis and reliability theory [16], as well as the prediction of position loss during DP operations using incident data and logistic regression [22]. Other studies have examined compass indication errors using shipboard measurements, spectral analysis and digital filtering [26]. Multiple sensor fault diagnosis has been investigated using detection and fault isolation methods for surface vessels [27]. The influence of multiple time-varying environmental factors on stochastic prognostics has also been considered [28]. Other studies have analysed human-related incidents during DP operations [29] and hazards affecting offshore DP systems, including adverse weather conditions, equipment failures and human factors [30]. Although these studies address DP reliability, compass indication errors, sensor faults, environmental variability and human factors, they do not jointly integrate operational gyrocompass alarm data, reliability estimation under different hydro-meteorological conditions and probabilistic oil spill risk assessment.

To address these gaps, a unified probabilistic framework is proposed that integrates stochastic modelling of hydro-meteorological variability, statistical parameter identification using empirical operational data, analysis of gyrocompass operational behaviour, reliability assessment, and consequence modelling. The proposed approach enables the evaluation of navigation system reliability in the context of offshore operational safety and environmental risk.

## 3. Dynamic Positioning System and Gyrocompass Operation

According to IMO guidelines [5], a Dynamic Positioning (DP) system comprises power, thruster and DP control subsystems, with the latter incorporating measurement and position-reference functions [4]. Reliable sensor inputs are critical because erroneous measurements may affect the performance of the DP control system.

DP systems may monitor the consistency of measurements from multiple sensors. Depending on the system configuration, discrepancies between sensor readings may trigger alarms, which can be recorded in the event log, or lead to the rejection of unreliable measurements [4,5]. Gyrocompasses provide heading information, and differences between their indications may therefore be used to identify potential measurement errors [31,32]. Such discrepancies do not necessarily indicate a physical failure of the gyrocompass.

Figure 2 illustrates the interactions between the DP operator and individual DP subsystems. The operator may control these subsystems and is responsible for continuously monitoring environmental conditions, system alarms, issued commands, and their execution. For example, the operator may directly adjust the settings of a reference system through the relevant control interfaces [4].

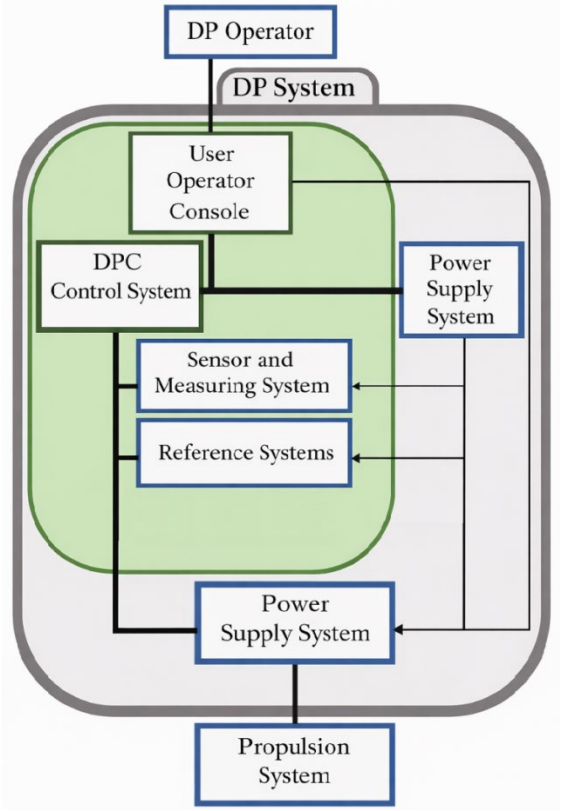



**Figure 2.** Structure of the Dynamic Positioning system and interactions between its subsystems, based on [4].

These mechanisms provide the technical context for the analysis presented below. The study focuses on the relationship between hydro-meteorological conditions and recorded gyrocompass alarms, followed by a reliability assessment and an evaluation of the role of gyrocompass reliability in the proposed risk model.

## 4. Research Methodology

This section contains a reliability model that integrates environmental disturbances with navigation sensor behaviour to estimate the likelihood of unstable conditions. The presented methodology may support improved reliability assessment and operational safety in offshore marine operations.

### *4.1. Environmental Disturbances Modelling*

To define hydro-meteorological states over a specified maritime area [33], a set of $a$ parameters, $w_1, w_2, \ldots, w_a$, is introduced, where $a \in \mathrm{N}$. It is further assumed that the admissible values of the $i$-th parameter $w_i$ belong to the interval $<b_i, d_i)$, $i = 1, 2, \ldots, a$. Each of these intervals can be partitioned into $n_i$ disjoint subintervals, where $n_i \in \mathrm{N}$.

The vector $[w_1, w_2, \ldots, w_a]$, describing the hydro-meteorological states, takes values from the set of points in the Cartesian product space

$$< b_1, d_1) \times < b_2, d_2) \times \ldots \times < b_a, d_a). \quad (1)$$

These sets are defined as the states of the hydro-meteorological process and are denoted by $hm_1, hm_2, \ldots, hm_w$ [13,34]. An example of a graphical interpretation of these states is presented in Figure 3.

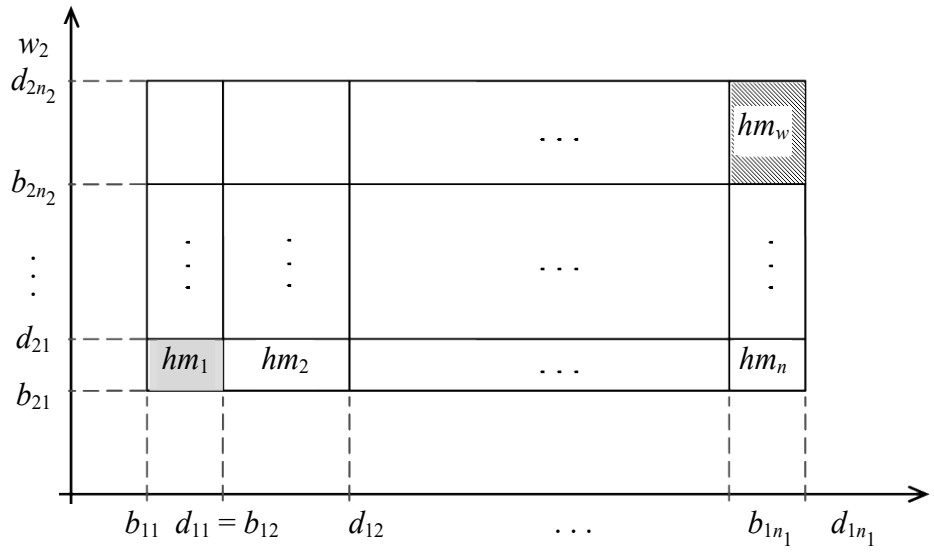



**Figure 3.** Graphical representation of the partitioning of the hydro-meteorological parameter space into discrete states.

It is assumed that, during operation, the system at any time $t \in \langle 0,\infty)$ can occupy one of $w$, $w \in \mathrm{N}$, hydro-meteorological states $hm_b$, $b = 1, 2, ..., w$. Accordingly, the hydro-meteorological process is denoted by $HM(t)$, a continuous-time stochastic process taking values in the discrete state space $HM = \{hm_1, hm_2, ..., hm_w\}$. A semi-Markov model [35–37] is assumed for this process.

In order to estimate the unknown parameters of the hydro-meteorological process [33,34], it is necessary to conduct an empirical study, including identification and collection of statistical data:

- Total observation time $\Theta$;
- Number $n(0)$ of observed realisations of the hydro-meteorological process at time $t = 0$;
- Initial state occurrences $n_b(0)$, $b = 1, 2, ..., w$, for $t = 0$, representing the number of realisations in which the process occupies states $hm_1, hm_2, ..., hm_w$

$$[n_b(0)] = [n_1(0), n_2(0), ..., n_w(0)] \tag{2}$$

where $n(0) = \sum_{b=1}^{w} n_b(0)$;

- Transition counts $n_{bl}$, $b, l = 1, 2, ..., w$, $b \neq l$ representing the number of transitions from state $hm_b$ to state $hm_l$

$$[n_{bl}] = \begin{bmatrix} n_{11}\ n_{12} \ldots n_{1w} \\ n_{21}\ n_{22} \ldots n_{2w} \\ \ldots \\ n_{w1}\ n_{w2} \ldots n_{ww} \end{bmatrix}; \tag{3}$$

- The residence (sojourn) time of the hydro-meteorological process in individual states during the observation period $\Theta$, including realisations $\theta_{bl}^k$, $k = 1, 2, ..., n_{bl}$, of the random conditional sojourn times $\Theta_{bl}$ representing the time the process remains in state $hm_b$, given that the next transition occurs to state $hm_l$, for each $b, l = 1, 2, ..., w$, $b \neq l$.

Considering the above, the following quantities can be defined and estimated:

- The vector

$$[q_b(0)]_{1\times w} = [q_1(0), q_2(0),..., q_w(0)]; \tag{4}$$

of initial probabilities $q_b(0) = P(HM(0) = hm_b) = \frac{n_b(0)}{n(0)}$, $b = 1, 2, \ldots, w$, at $t = 0$;

- The transition probability matrix:

$$[q_{bl}] = \begin{bmatrix} q_{11}\ q_{12} \cdots q_{1w} \\ q_{21}\ q_{22} \cdots q_{2w} \\ \cdots \\ q_{w1}\ q_{w2} \cdots q_{ww} \end{bmatrix}, \tag{5}$$

where transition probabilities between states $hm_b$ and $hm_l$ are defined as

$$q_{bl} = \frac{n_{bl}}{n_b} = \frac{n_{bl}}{\sum_{\substack{j=1 \\ j\neq b}}^{w} n_{bj}}, \quad b \neq l, \tag{6}$$

and $n_b$ denotes the total number of occurrences of state $hm_b$, $b = 1, 2, \ldots, w$, during the observation period $\Theta$.

A random sample $\left(\Theta_{bl}^1, \Theta_{bl}^2, ..., \Theta_{bl}^{n_{bl}}\right)$, of size $n_{bl}$ with realisations $\left(\theta_{bl}^1, \theta_{bl}^2, ..., \theta_{bl}^{n_{bl}}\right)$, is then obtained. Based on this sample, an empirical histogram may be constructed. Subsequently, statistical hypotheses concerning the form of the unknown distributions of the sojourn times $\Theta_{bl}$ can be verified for fixed $b,l \in \{1, 2, ..., w\}$, $b \neq l$.

### *4.2. Reliability Assessment Methodology*

In this subsection, a two-state approach to the reliability analysis of non-repairable objects [38,39] is adopted. This approach assumes that the analysed object may occupy only one of two reliability states, i.e., it is either operational (functional) or failed (non-operational). The time to failure (TTF), $T$, is assumed to be a non-negative continuous random variable, and the reliability function is defined as follows [40–43]:

$$R(t) = P(T \geq t),\ t \in (0, \infty). \tag{7}$$

The non-repairable approach is adopted here as a simplification for modelling the time to an observed alarm event. The model describes the probability of remaining free from such an event over a specified time interval and does not explicitly represent subsequent repairs or restoration of functionality. Therefore, the analysed gyrocompasses are not assumed to be physically non-repairable. The approach is used to estimate alarm-related reliability characteristics rather than the complete operational availability of repairable equipment.

The analysed object is characterised by its failure intensity (hazard rate) function, defined as

$$\lambda(t) = \lim_{\Delta t \to 0} \frac{R(t) - R(t + \Delta t)}{\Delta t R(t)} = \frac{f(t)}{R(t)}, \tag{8}$$

where $f(t)$ denotes the probability density function of the time to failure $T$.

Furthermore, it is assumed that the distributions of the sojourn times of system components $E_i$, $i = 1, 2, \ldots, n$, depend on the states of the hydro-meteorological process $HM(t)$ [36,44–46]. This allows the influence of changing environmental conditions to be reflected in the reliability characteristics of system components.

The conditional reliability function of a component is then defined as:

$$R_i^{(b)}(t) = P\left(T_i^{(b)} \geq t \middle| HM(t) = hm_b\right),\ t \in <0, \infty),\ i = 1, 2, \ldots, n,\ b = 1, 2, \ldots, w. \tag{9}$$

The function $R_i^{(b)}(t)$ represents the conditional probability that the time to failure $T_i^{(b)}$ of component $E_i$ is not shorter than $t$, given that the hydro-meteorological process $HM(t)$ is in state $hm_b$.

To determine the system reliability function while accounting for both component reliability variability and the influence of the hydro-meteorological process, conditional reliability functions are first evaluated, followed by the unconditional system reliability function [46], defined as:

$$\boldsymbol{R}^{(b)}(t) = P\left(T^{(b)} \geq t \middle| HM(t) = hm_b\right), \tag{10}$$

where $\boldsymbol{R}^{(b)}(t)$ denotes the conditional probability that the system time to failure $T^{(b)}$ is not shorter than $t$, given that the hydro-meteorological process is in state $hm_b$.

The unconditional reliability function of the system is defined as:

$$\boldsymbol{R}_S(t) = P(T > t) = \sum_{b=1}^{w} q_b(t)\boldsymbol{R}^{(b)}(t), \tag{11}$$

where $T$ denotes the unconditional system lifetime (TTF), and $\boldsymbol{R}^{(b)}(t)$ is defined by Equation (10).

If the observation time $\Theta$ is sufficiently large, the time-dependent probabilities $q_b(t)$ may be approximated by their limit values [13,36,37], determined from

$$q_b = \lim_{t\to\infty} q_b(t) = \frac{p_b \cdot M_b}{\sum_{l=1}^{w}[p_l \cdot M_l]}, \tag{12}$$

where

$$\begin{cases} [p_1, p_2, \ldots, p_w] = [p_1, p_2, \ldots, p_w]\,[q_{bl}] \\ \sum\limits_{l=1}^{w} p_l = 1, \end{cases} \tag{13}$$

$$M_b = E[\Theta_b] = \sum_{l=1}^{w}\left[q_{bl}\left(\int_0^{\infty} t \cdot h_{bl}(t)dt\right)\right], \tag{14}$$

and the following approximation is obtained:

$$\boldsymbol{R}_S(t) \cong \sum_{b=1}^{w} q_b \boldsymbol{R}^{(b)}(t). \tag{15}$$

For clarity and consistency throughout the reliability assessment, all variables, parameters, and indicators associated with the gyrocompass system will be denoted using the subscript $G$.

### 4.3. Hierarchical Probabilistic Risk Model Linking Gyrocompass Reliability to Environmental Risk

To investigate the quantitative relationship between hydro-meteorological variability, system performance and environmentally critical outcomes, the estimated reliability characteristics are incorporated into a hierarchical probabilistic risk model. In this context, the gyrocompass constitutes a key component within the shipborne navigation suite, and its degradation or failure may initiate a cascade of events leading to loss of situational awareness and, ultimately, maritime accidents.

For the considered event sequence, the oil spill probability is estimated using the following product under the adopted simplifying assumptions [9,16,20,47]:

$$P_{oil\ spill}(t) = P_{Gf}(t) \cdot P_{Lp|Gf}\ (t) \cdot P_{A|Lp}(t) \cdot P_{S|A}(t), \tag{16}$$

where $G_f(t)$ denotes gyrocompass failure, $L_p(t)$ represents loss of reliable position or heading information, $A$ corresponds to an accident scenario (e.g., grounding or collision), and $S$ is interpreted as an accident resulting in an oil spill.

For mutually exclusive gyrocompass failure scenarios, this formulation can be extended to incorporate multiple failure modes and operational contexts [9,34,48–51]:

$$P_{oilspill}(t) = \sum_{i=1}^{n}\left[P_{G_{f,i}}(t)\cdot P_{L_p|G_{f,i},C}(t)\cdot P_{A|L_p,E}(t)\cdot P_{S|A}(t)\right], \quad (17)$$

where $G_{f,i}(t)$ represents the $i$-th gyro failure mode (e.g., drift, bias instability, total outage), $C$ denotes operational conditions (traffic density, navigation complexity), $E$ represents environmental conditions (weather, sea state), and $S$ denotes the occurrence of an oil spill following an accident (dependent on hull integrity, cargo type, and impact energy). Alternatively, it can be presented as (see Section 4.2):

$$P_{oil\ spill}(t) = P(T_G \le t)\cdot P(T_{Lp} \le t|T_G \le t)\cdot P(T_A \le t|T_{Lp} \le t)\cdot P(S|T_A \le t). \quad (18)$$

The transition from gyro failure to loss of position can be further characterised through a conditional performance degradation model. For instance, the conditional probability is given by

$$P_{Lp|Gf}(t) = \frac{P(L_p(t) \cap G_f(t))}{P(G_f(t))} = f(\Delta\theta, t_r, H), \quad (19)$$

where $\Delta\theta$ is heading error magnitude, $t_r$ is the mean response time to detect and correct the fault, and $H$ denotes human operator performance. This emphasises that the propagation of failure is not purely technical but socio-technical in nature [52,53].

The probability of an accident conditional on loss of position can be expressed using the joint probability of these events and modelled for the considered operational scenario using an exponential traffic-riskexpression:

$$P_A|_{Lp}(t) = \frac{P(A(t) \cap L_p(t))}{P(L_p(t))} = 1 - \exp(-D(t)\cdot T_e\cdot\beta(t)), \quad (20)$$

where $D$ denotes traffic density, $T_e$ is the exposure time under degraded navigation conditions, and $\beta$ is a traffic risk coefficient adopted for the considered operational scenario, informed by maritime traffic risk modelling literature.

Finally, the probability that an accident results in an oil spill can be linked to impact energy $E_{impact}$ (collision or grounding energy) and structural resistance:

$$P_S|_A(t) = \frac{P(S(t) \cap A(t))}{P(A(t))} = P_{Eimpact>Ecrit}(t), \quad (21)$$

with $E_{crit}$ representing the threshold energy required to breach cargo tanks. This term may be evaluated using structural reliability approaches [54,55].

In the risk assessment, an additional scaling coefficient $k_{S|A}$ may be introduced to account for factors affecting oil release after an accident that are not explicitly represented by the impact–resistance threshold. This coefficient allows the threshold-exceedance probability in Equation (21) to be adjusted for the conditions considered in the risk model.

The proposed hierarchical probabilistic structure integrates component-level reliability, navigation system performance and operational conditions to estimate environmental risk. Such formulations are particularly suitable for coupling with Bayesian networks or dynamic fault trees, allowing both predictive analysis and real-time risk monitoring in modern e-navigation systems.

## 5. Case Study: Time-Dependent Oil Spill Risk Driven by a Platform Supply Vessel's Gyrocompass Reliability

This case study demonstrates the practical application of the proposed reliability-risk framework (Section 4) by linking the Platform Supply Vessel's gyrocompass reliability

characteristics with a probabilistic model of accident occurrence and environmental consequences. The objective is to quantify how degradation in a critical navigation component propagates through the socio-technical system and contributes to environmental risk over time. For the purpose of this case study, values representing moderate operational conditions were adopted, corresponding to partial automation and realistic response delays. This results in a non-negligible probability of navigation degradation following gyro failure, particularly in complex traffic environments.

The reliability characteristics of the gyrocompass, including alarm-related time distribution and statistical moments, were estimated from real operational data, taking into account hydro-meteorological conditions recorded in the deck logs [56]. These results describe the observed alarm-related behaviour of the navigation equipment under the recorded operational and hydro-meteorological conditions. However, the available data do not allow individual physical failure mechanisms or age-related wear effects to be identified separately.

To evaluate the impact of redundancy, both a single-gyro configuration and a three-unit parallel system were considered. The latter corresponds to standard redundancy practices in modern maritime navigation, where multiple independent heading sources are used to improve robustness. As expected, redundancy significantly extends the effective operational lifetime and reduces the probability of system-level failure within a given time horizon.

### *5.1. Platform Supply Vessels*

Platform Supply Vessels (PSVs) are designed to transport supplies and equipment to offshore installations (Figure 4). Their operational characteristics, including a large cargo deck and superstructure, are relevant to vessel stability and motion in waves, wind and current.

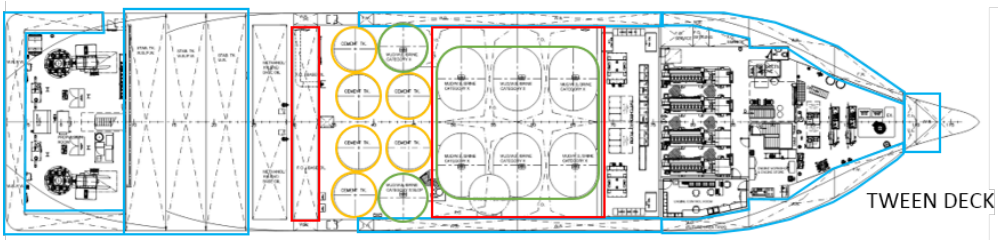



**Figure 4.** Example arrangement of tanks on a PSV: blue—water tanks, red—fuel tanks, green—brine/drilling fluid tanks, yellow—cement/barite tanks [56].

A vessel at sea has six degrees of freedom: three rotational motions (roll, pitch and yaw) and three translational motions(surge, sway and heave)(Figure 5). For surface vessels equipped with Dynamic Positioning (DP) systems, maintaining position and heading requires continuous measurements and corrective actions in response to external forces (see Section 3). When environmental conditions exceed the vessel's operational capabilities, maintaining the required position or heading may become difficult, and the DP system may generate alarms [57,58].

The present study focuses on the gyrocompass measurements used in this process and their relationship with hydro-meteorological conditions.

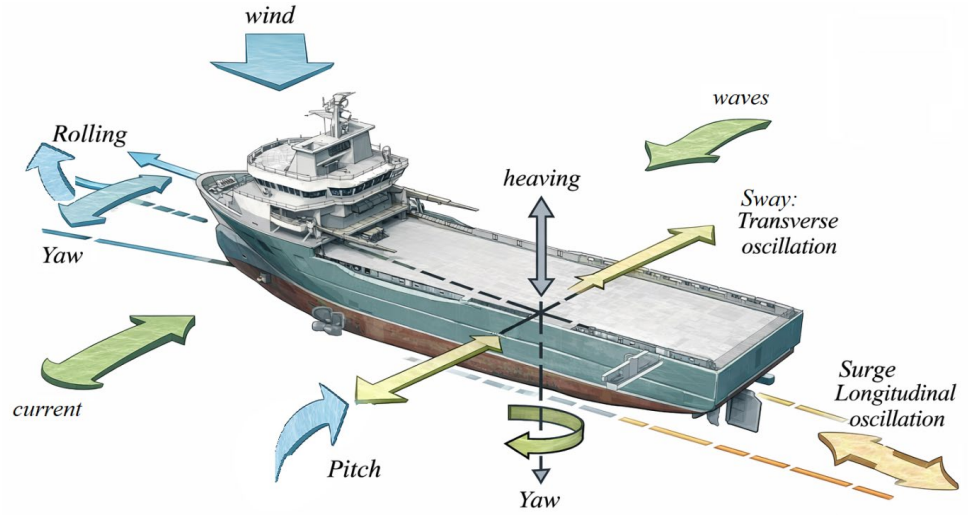



**Figure 5.** Vessel motions under the influence of waves, wind, and current, based on [58].

### 5.2. Troms Capella PSV—Technical Data and Equipment

The reliability study was conducted on board *Troms Capella*, a Platform Supply Vessel (PSV) operating in the offshore sector (Figure 6). The vessel was built in 2011 and has an overall length of 88.1 m, a beam of 19 m and a deadweight of 4660 t [59]. Its large open cargo deck and superstructure are characteristic of vessels designed to support offshore operations.

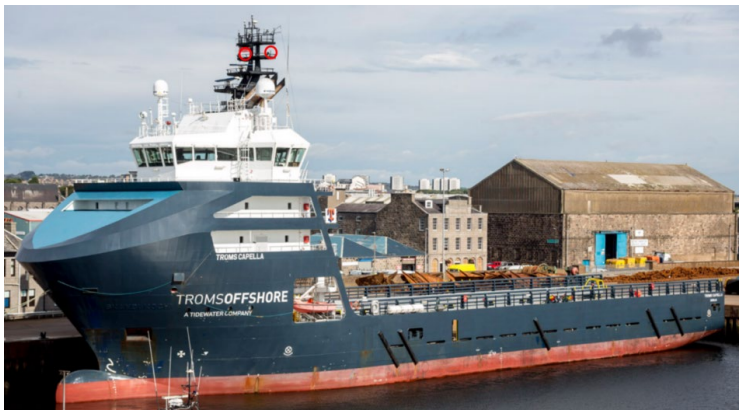



**Figure 6.** *Troms Capella* in the port of Aberdeen on 23.08.2019 [56].

The vessel has a diesel-electric propulsion system and is equipped with a Kongsberg K-Pos DP-21 system (DP Class 2). Its navigation and positioning equipment includes three gyrocompasses, three Motion Reference Units (MRUs), two independent DGPS systems and additional positioning reference systems (Tables 1 and 2) [59].

**Table 1.** Navigational equipment of the vessel *Troms Capella*, based on [59].

| Equipment | Quantity |
|---|---|
| Radars | 2 |
| Echo sounder | 1 |
| Gyrocompasses | 3 |
| Doppler log | 1 |
| Radios | 8 x VHF |
| Satellite communication | V-Sat |

**Table 2.** Specialised equipment of the vessel *Troms Capella*, based on [59].

| Equipment | Specification |
|---|---|
| Dynamic Positioning system | DP Class 2 (Kongsberg K-Pos DP-21) |
| Reference systems | 3 × MRU<br>2 × DGPS<br>1 × Laser-based<br>1 × RADius |
| Drilling fluid recirculation and tank cleaning system | Available |
| Agitators | 6 |

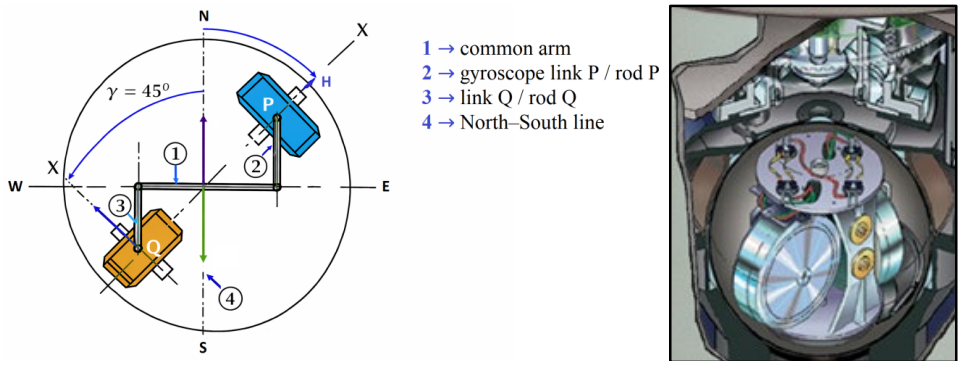
The three gyrocompasses are installed in the forward instrument room, on an intermediate deck between the officers' deck and the bridge (Figure 7). Their location relative to the vessel's centre of flotation is relevant because vessel motion may affect the operating conditions of the gyrocompass damping system. The following section describes the gyrocompass configuration and the maintenance events considered in the reliability analysis.




**Figure 7.** Bridge view from the aft deck of the vessel *Troms Capella* [56].

### *5.3. Troms Capella PSV—Gyrocompasses*

*Troms Capella* is equipped with three Anschütz Standard 22 gyrocompasses. Each unit contains a measuring element immersed in compass fluid, whose temperature must be maintained within the range of 49–52°C to ensure the required operating conditions [60]. A heater and circulation pump maintain the fluid temperature and circulation. The follow-up system compensates for vessel motion and supports the transmission of heading information. The arrangement and main components of the gyrocompass are shown in Figures 8–10.




(**a**) (**b**)

**Figure 8.** Arrangement of gyroscopes in the measuring element: (**a**) based on [61] (p. 47); (**b**) based on [60].

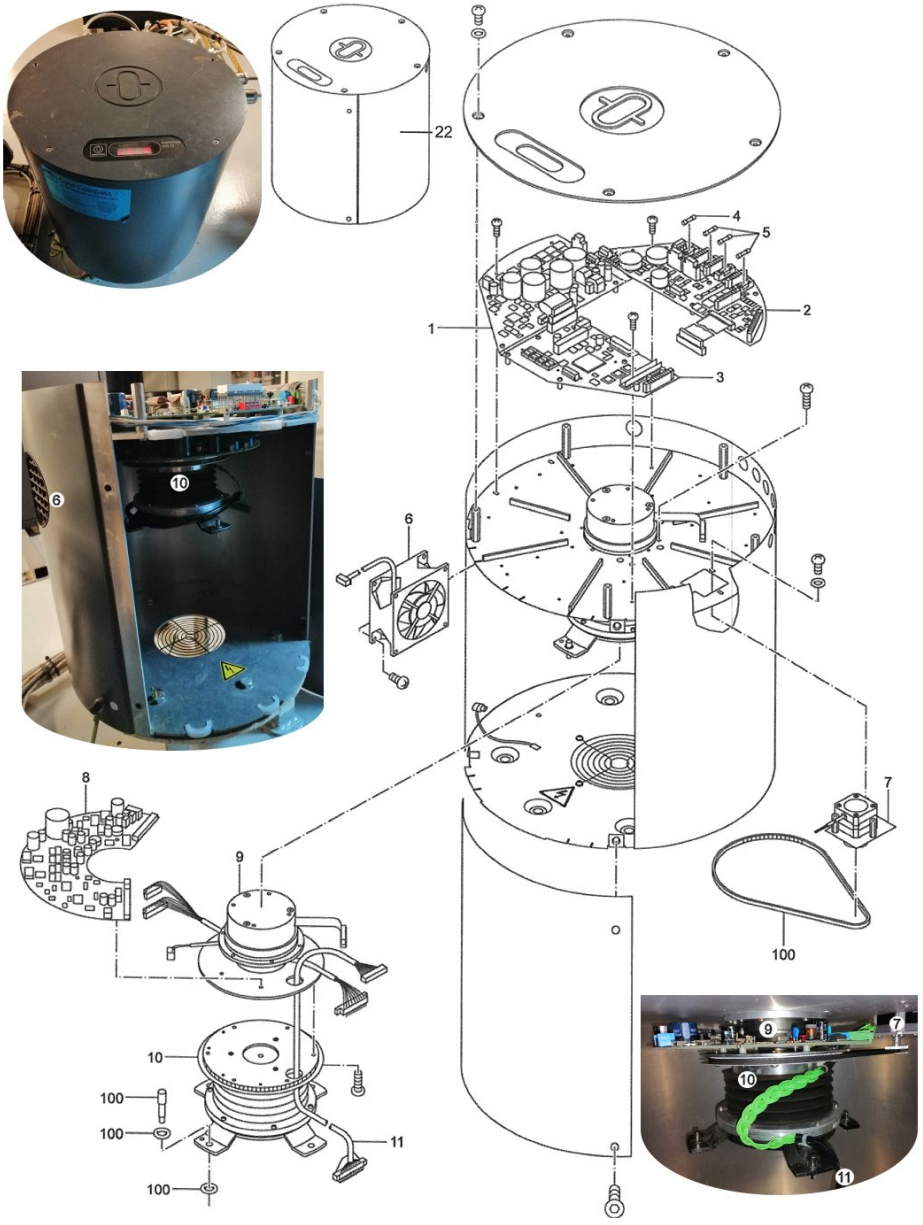



**Figure 9.** Components of the STD 22 gyrocompass [56].

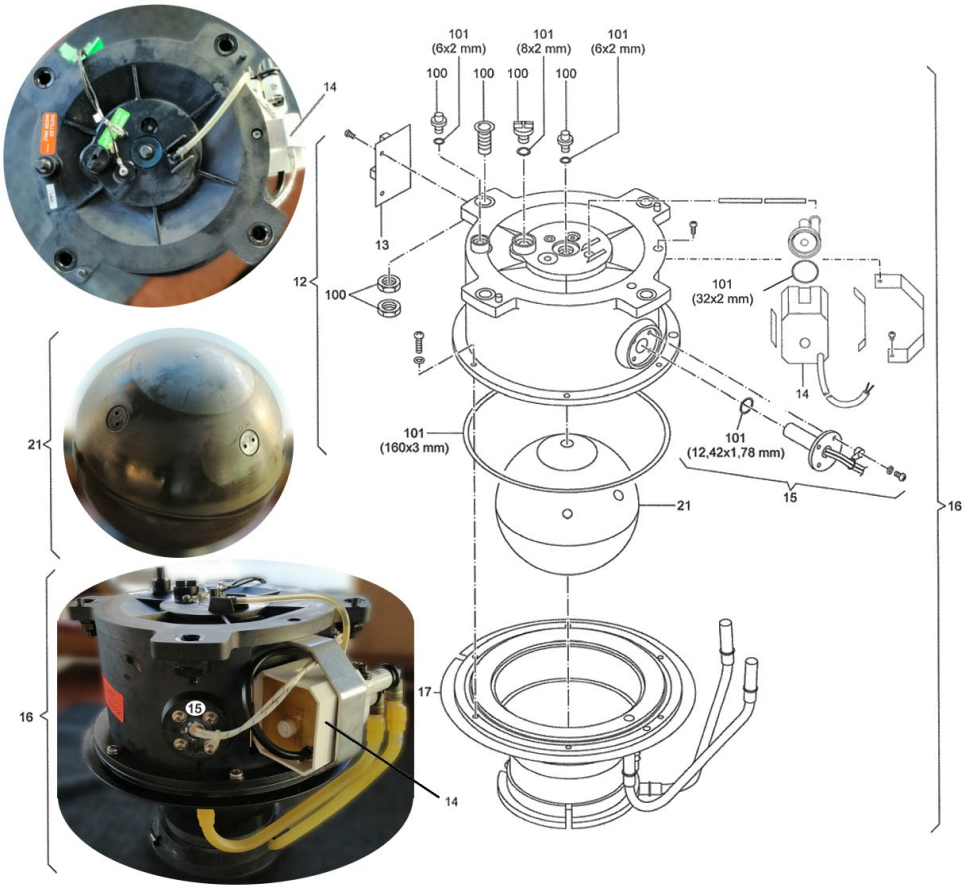



**Figure 10.** Components of the follow-up sphere of the STD 22 gyrocompass [56].

According to the service records, all three gyro spheres were replaced in February 2018. The analysed operational data cover the period from 1 January 2019 to 15 June 2020.During the study period, several maintenance interventions were recorded, including pump motor replacement and adjustment of gyrocompass alignment (see Table 3 and Appendix B). The gyro sphere in gyrocompass no. 1 was replaced on 29 November 2019, and the sphere in gyrocompass no. 2 was replaced on 27 February 2020 [56,62–64].

**Table 3.** Summary of key gyrocompass maintenance actions, based on [62–64].

| Gyrocompass | Gyro Sphere Replacement | Maintenance and Inspection |
|---|---|---|
| 1 | 02.2018<br>29.11.2019 | 05.11.2019 |
| 2 | 02.2018<br>27.02.2020 | 24.10.2019 |
| 3 | 02.2018 | 24.10.2019 |

During the service intervention on 24 October 2019, a low compass-fluid-level alarm history was noted for gyrocompass no. 2. At the subsequent intervention on 5 November 2019, a tendency for this unit to generate DP alarms associated with heading deviations from the median of the three gyrocompasses was observed, and continuous monitoring was recommended. The same intervention included maintenance of gyrocompass no. 1 and an alignment adjustment of gyrocompass no. 3.

These maintenance records are important when interpreting the alarm data because repairs and component replacements may affect the subsequent operational behaviour of individual units. However, a recorded heading-deviation alarm does not by itself establish that a physical failure occurred. The reliability analysis therefore uses the available alarm records as observations of operational behaviour, while the maintenance history provides additional context for their interpretation.

### *5.4. Identification of a Varying Hydro-Meteorological Stochastic Process*

The operating area of the analysed vessel is a key factor influencing the characteristics of the collected hydro-meteorological data. The approximate area of operation is presented in Figure 11.

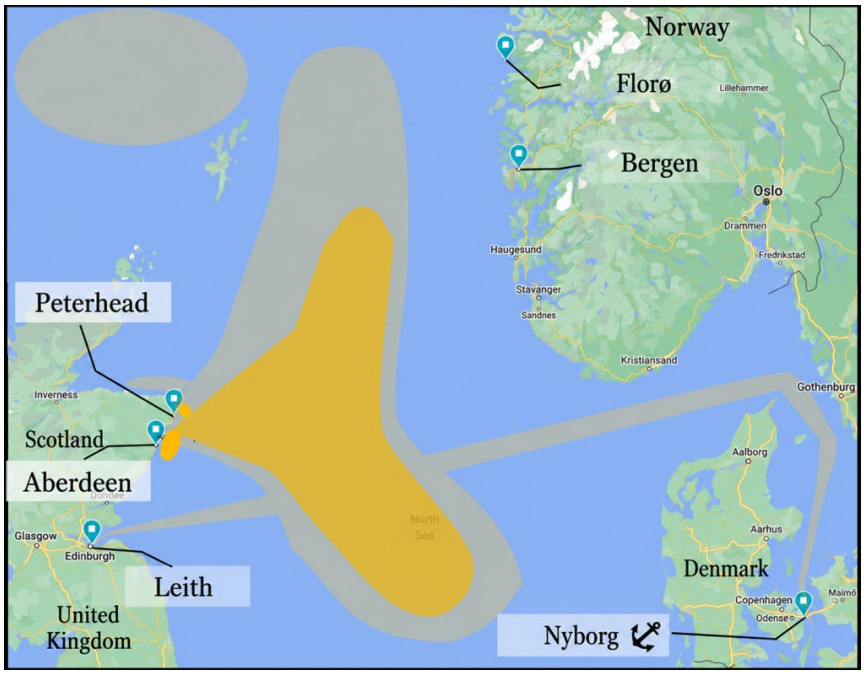



**Figure 11.** Map showing the approximate operational areas of the vessel *Troms Capella* during the study period, based on Google Maps.

Wind speed and wave height data were obtained from the deck logs of the vessel *Troms Capella* and are presented in the first three columns of Table 4. The dataset covers the period from 1 January 2019 00:00 to 15 June 2020 21:00, with observations recorded at three-hour intervals.

**Table 4.** Fragment of the hydro-meteorological observation dataset.

| Date | Wind Speed [°B] | Wave Height [m] | Comment | Hydro-Meteorological State | Duration [Days] | Transition |
|---|---|---|---|---|---|---|
| … | … | … | … | … | … | … |
| 2019-01-12 03:00 | 4 | 5.5 | | $hm_{M1}$ | 0.375 | $hm_{M1} \rightarrow hm_{M2}$ |
| 2019-01-12 06:00 | 7 | 6 | | $hm_{M2}$ | 0.125 | $hm_{M2} \rightarrow hm_{M1}$ |
| 2019-01-12 09:00 | 6 | 3 | | $hm_{M1}$ | 0.125 | $hm_{M1} \rightarrow hm_{L1}$ |
| 2019-01-12 12:00 | 3 | 0 | harbour | $hm_{L1}$ | 0.125 | $hm_{L1} \rightarrow hm_{M1}$ |
| 2019-01-12 15:00 | 5 | 4 | departure | $hm_{M1}$ | | |
| 2019-01-12 18:00 | 4.5 | 4.5 | | $hm_{M1}$ | | |

**Table 4.** *Cont.*

| Date | Wind Speed [°B] | Wave Height [m] | Comment | Hydro-Meteorological State | Duration [Days] | Transition |
|---|---|---|---|---|---|---|
| 2019-01-12 21:00 | 4 | 5 | | $hm_{M1}$ | | |
| 2019-01-13 00:00 | 5 | 5 | | $hm_{M1}$ | | |
| 2019-01-13 03:00 | 4 | 4 | | $hm_{M1}$ | | |
| 2019-01-13 06:00 | 3.5 | 3.5 | | $hm_{M1}$ | | |
| 2019-01-13 09:00 | 3 | 3 | | $hm_{M1}$ | 0.875 | $hm_{M1}\rightarrow hm_{M2}$ |
| 2019-01-13 12:00 | 7 | 3 | | $hm_{M2}$ | | |
| 2019-01-13 15:00 | 7 | 3 | | $hm_{M2}$ | 0.25 | $hm_{M2}\rightarrow hm_{L2}$ |
| 2019-01-13 18:00 | 7 | 0 | harbour | $hm_{L2}$ | | |
| 2019-01-13 21:00 | 7 | 0 | | $hm_{L2}$ | | |
| 2019-01-14 00:00 | 7 | 0 | | $hm_{L2}$ | | |
| 2019-01-14 03:00 | 7 | 0 | | $hm_{L2}$ | 0.5 | $hm_{L2}\rightarrow hm_{L1}$ |
| 2019-01-14 06:00 | 5 | 0 | | $hm_{L1}$ | | |
| 2019-01-14 09:00 | 4 | 0 | | $hm_{L1}$ | | |
| … | … | … | … | … | … | … |

Based on wind speed and wave height, six hydro-meteorological states ($w = 6$) were defined (Figure 12), where the letters L, M, and H denote low, medium, and high levels of wave height, respectively, while the subscripts distinguish the corresponding wind speed categories. Each observation was assigned to one state using the classification criteria in Figure 12.

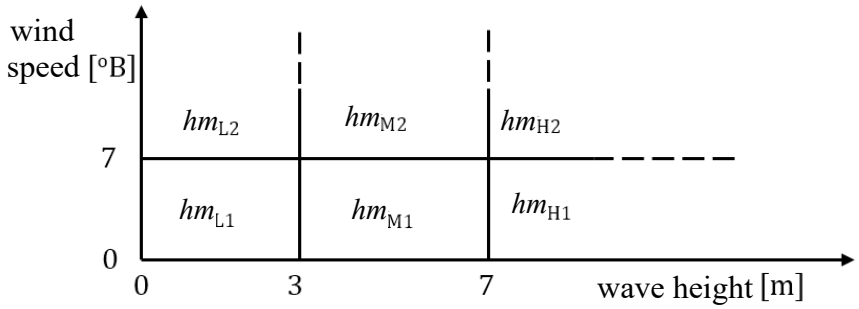



**Figure 12.** Hydro-meteorological states affecting the gyrocompass.

The six hydro-meteorological states were defined using the two environmental variables available in the deck-log records: wind intensity expressed on the Beaufort scale, and significant wave height expressed in metres. The thresholds of 3 m and 7 m for wave height and Beaufort force 7 for wind conditions were adopted as practical classification limits for distinguishing mild, moderate and severe operating conditions in the analysed case study. These thresholds were used as modelling boundaries for discretising the observed environmental conditions into a finite state space. They should therefore be interpreted as operational classification limits adopted for the present analysis rather than universal physical thresholds applicable to all offshore vessels and sea areas.

The duration of each state was calculated and expressed in days; thus, 0.125 corresponds to three hours. Transitions between consecutive states were also identified. For example, a transition from $hm_{M1}$ to $hm_{M2}$ was denoted as $hm_{M1}\rightarrow hm_{M2}$. The resulting state sequence was used to estimate the parameters of the hydro-meteorological process required by the semi-Markov model:

- The vector of initial state occurrences (at midnight):

$$[n_b(0)] = [277, 140, 0, 10, 31, 7]; \quad (22)$$

- The matrix of transition counts according to (3):

$$[n_{bl}] = \begin{bmatrix} 0 & 14302914 & 0 \\ 141 & 0 & 0\,4\,89\ 2 \\ 0 & 1 & 0\,0\ 0\ 0\ 0 \\ 27 & 3 & 0\,0\ 8\ 0 \\ 17 & 80 & 0\,5\ 0\,20 \\ 1 & 9 & 1\,0\,11\,0 \end{bmatrix}; \quad (23)$$

- The vector of total transitions representing exits from state $hm_b$:

$$[n_b] = [186,\ 236,\ 1,\ 38,\ 122,\ 22]; \quad (24)$$

- The initial probabilities at time $t = 0$ given as a vector, as defined in Equation (4):

$$[q_b(0)] = [0.596,\ 0.301,\ 0,\ 0.021,\ 0.067,\ 0.015]; \quad (25)$$

- The transition probability matrix between states using Equations (5) and (6):

$$[q_{bl}] = \begin{bmatrix} 0 & 0.76882 & 0 & 0.15591 & 0.07527 & 0 \\ 0.59746 & 0 & 0 & 0.01695 & 0.37712 & 0.00847 \\ 0 & 1 & 0 & 0 & 0 & 0 \\ 0.71053 & 0.07895 & 0 & 0 & 0.21052 & 0 \\ 0.13934 & 0.65574 & 0 & 0.04098 & 0 & 0.16394 \\ 0.04545 & 0.40909 & 0.04546 & 0 & 0.5 & 0 \end{bmatrix}; \quad (26)$$

- Matrix $[h_{bl}(t)]$, $t \in \langle 0,\infty)$, of conditional probability density functions of sojourn times $\Theta_{bl}$, $b$,$l = 1, 2, \ldots, 6$, whose mean values are presented in the next subsection; see Equation (27).

The calculations were performed in Microsoft Excel using custom VBA macros to process the 3928 records, including observations excluded from the calculation of the effective exposure time. This procedure provided the state-transition counts and sojourn times used in the subsequent modelling (Appendix A, Figures A1 and A2).

### *5.5. Prediction of Changes in the Hydro-Meteorological Process*

The data described in Section 5.4 were used to estimate the parameters of the semi-Markov model defined in Section 4.1. The analysis included the transition probabilities between hydro-meteorological states and the distributions of state sojourn times.

Candidate distributions were fitted to the observed sojourn times for individual transitions. Exponential, gamma, chimney and empirical distributions were used, depending on the observations and the results of statistical goodness-of-fit assessment. The estimated mean sojourn times were then used to calculate the long-run proportion of time spent in each state and the corresponding expected durations over a 365-day period.

The expected values $M_{bl} = E[\Theta_{bl}]$ of the conditional sojourn times for $b$, $l = 1, 2, \ldots, 6$, $b \neq l$, are calculated from the statistically fitted distributions:

$$[M_{bl}] = \begin{bmatrix} 0 & 1.42 & 0 & 2.96 & 1.58 & 0 \\ 0.53 & 0 & 0 & 0.28 & 0.55 & 0.19 \\ 0 & 0.125 & 0 & 0 & 0 & 0 \\ 0.26 & 0.12 & 0 & 0 & 0.22 & 0 \\ 0.25 & 0.37 & 0 & 0.22 & 0 & 0.28 \\ 0.625 & 0.38 & 0.125 & 0 & 0.12 & 0 \end{bmatrix}. \quad (27)$$

The mean sojourn times $M_b$, calculated using Equation (14), are:

$$M_1 = 1.672;\ M_2 = 0.53;\ M_3 = 0.125;\ M_4 = 0.241;\ M_5 = 0.332;\ M_6 = 0.25. \quad (28)$$

Using these characteristics and Equations (12)–(14), the limit transient probabilities were obtained:

$$q_1 = 0.633,\ q_2 = 0.254,\ q_3 = 0.00025 \approx 0,\ q_4 = 0.019,\ q_5 = 0.082,\ q_6 = 0.012. \quad (29)$$

For a sufficiently long observation time, e.g., $\Theta = 365$ days, the total expected time spent in each state is:

$$M_b = q_b\Theta = 365q_b,\ b = 1, 2, ..., 6, \quad (30)$$

which gives

$$M_1 \approx\ 231.05,\ M_2 = 92.71,\ M_3 = 0,\ M_4 \approx\ 6.94,\ M_5 = 29.93,\ M_6 = 4.38. \quad (31)$$

The resulting parameters describe the hydro-meteorological conditions represented in the operational data. Their interpretation is subject to the limitations of the observation period and the very short exposure duration of state $hm_{\mathrm{H1}}$, which occurred only once and lasted 0.125 days (3 h). Although all six predefined states were retained in the model, the available observations were insufficient to characterise state $hm_{\mathrm{H1}}$ reliably.

### *5.6. Reliability of a Gyrocompass System*

The reliability analysis was based on two data sources: deck-log records of wind speed and wave height, covering the period from 1 January 2019 to 15 June 2020, and alarm records from the vessel's DP system. The latter included events associated with deviations between gyrocompass readings and the median of the available measurements. An example page of this log is shown in Figure 13.

The recorded events represent heading-deviation alarms rather than independently confirmed physical failures. Accordingly, the observed times are treated as times to alarm occurrence in the operational data. They should not be interpreted as direct measurements of the time to physical failure of a gyrocompass. This distinction is important when interpreting the reliability estimates derived from the alarm records.

The 2° threshold represents the heading-deviation criterion used for alarm generation by the DP system on the analysed vessel. It refers to the difference between an individual gyrocompass reading and the median of the available heading measurements. Exceeding this threshold indicates a measurement discrepancy requiring attention but does not necessarily mean that the gyrocompass has lost its functionality. The DP system may continue to operate using the remaining heading measurements. Actual loss of reliable heading information would involve a situation in which the available measurements could no longer provide a sufficiently reliable heading reference for the DP system. The recorded alarms were therefore used as indicators of operational deviations rather than as confirmed events of complete functional failure.

The alarm data (Table 5) were grouped and filtered to reduce repeated records associated with state transitions and to retain events relevant to the three gyrocompasses. The resulting dataset contained 190 alarm groups with a total weight of 2317, representing the total number of recorded alarm occurrences within these groups. Following the additional selection described in the data-processing procedure, 96 alarm records, with a combined weight of 1148, were included in the summary presented in Table 6. The selected alarm records are also illustrated in Figures A3 and A4 (Appendix B). The event weights and gyro codes (classified in Appendix B, Figure A5) were used to characterise the selected observations.

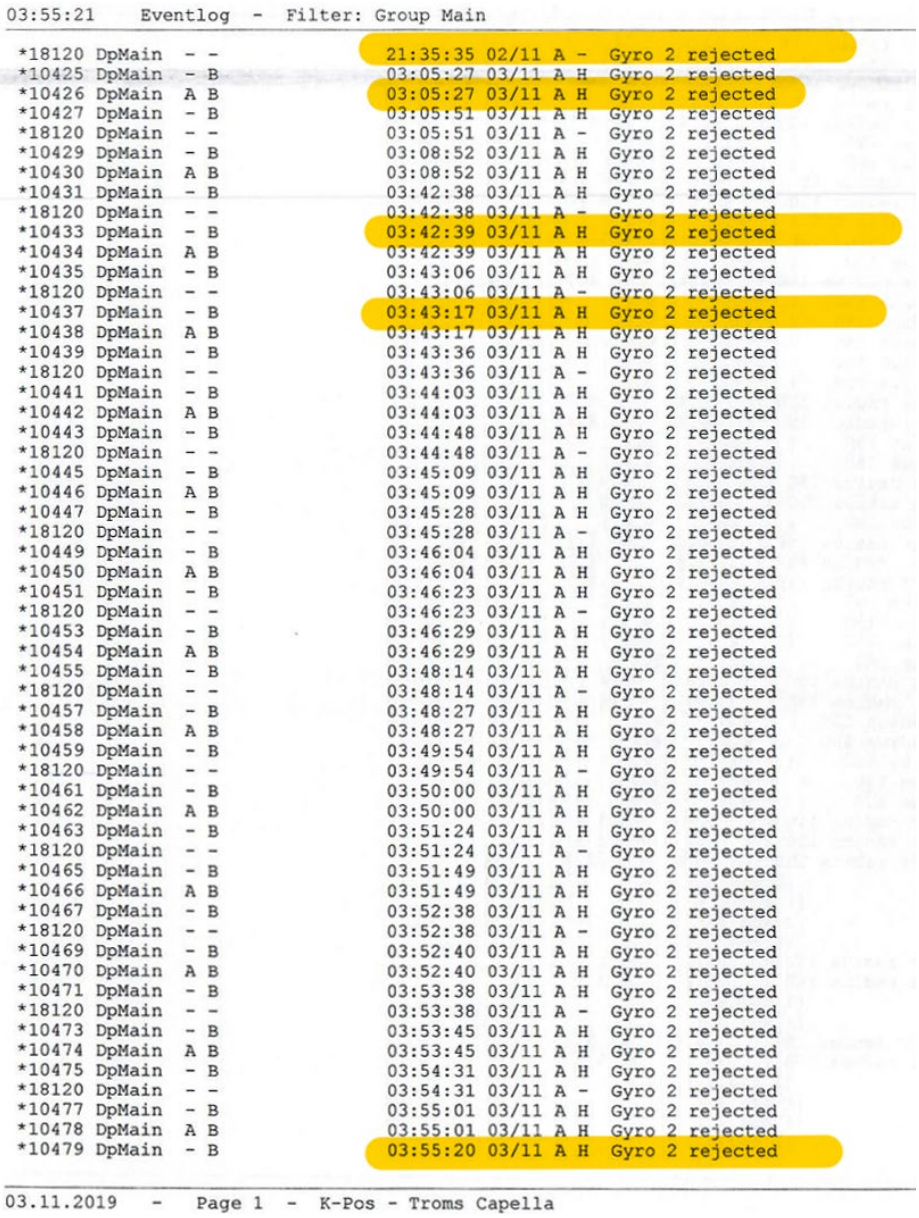



**Figure 13.** Example page from the event log [56].

**Table 5.** Fragment of the table summarising hydro-meteorological conditions and system alarms.

| No. | Date and Time of Alarm | Previous State | State | Time to Alarm Occurrence [hh:mm] | Weight | Gyro Code |
|---|---|---|---|---|---|---|
| … | … | … | … | … | … | … |
| 190 | 2019-01-10 15:15 | $hm_{L1}$ | $hm_{M1}$ | 3:15 | 5 | 2 |
| 189 | 2019-01-11 19:36 | $hm_{M2}$ | $hm_{M1}$ | 1:36 | 16 | 2 |
| 187 | 2019-01-12 19:27 | $hm_{M2}$ | $hm_{M1}$ | 7:27 | 5 | 2 |
| 184 | 2019-03-29 23:00 | $hm_{L1}$ | $hm_{M1}$ | 8:00 | 5 | 2 |
| 183 | 2019-03-30 12:32 | $hm_{M2}$ | $hm_{H2}$ | 3:32 | 5 | 2 |
| 182 | 2019-03-30 21:02 | $hm_{H2}$ | $hm_{M1}$ | 3:02 | 5 | 2 |
| 180 | 2019-04-24 01:57 | $hm_{M2}$ | $hm_{M2}$ | 13:57 | 5 | 2 |
| 178 | 2019-04-24 15:59 | $hm_{M2}$ | $hm_{M1}$ | 3:59 | 2 | 40 |
| 177 | 2019-06-12 07:52 | $hm_{L1}$ | $hm_{H2}$ | 1:52 | 13 | 5 |
| … | … | … | … | … | … | … |

**Table 6.** Summary of results.

| Number of Days Considered | Number of Selected Alarm Records | Average Hydro-Meteorological Conditions |
|---|---|---|
| 465 days | 96 | Wind 4 [°B]<br>Wave height 2 [m] |

The total duration of available data classified into the six hydro-meteorological states was 464.5 days, rounded to 465 days in Table 6. Periods marked as "no data" were excluded from this total.

The time to alarm data $T_i^{(b)}$, $i$ = 1,2,3, $b$ = 1, 2, ..., 6, were modelled using exponential distributions. This assumption simplifies the analysis by treating the event process as memoryless; however, it does not account explicitly for ageing, maintenance interventions or changes in equipment condition. The resulting estimates should therefore be interpreted as estimates of the time to alarm occurrence, rather than as direct estimates of the time to physical failure of the gyrocompasses.

The operational records also include maintenance interventions and replacements of gyrocompass components during the observation period (Section 5.3). These interventions may have influenced subsequent alarm occurrence. However, repair and replacement processes were not explicitly incorporated into the adopted reliability model, and the analysis does not distinguish separate pre-maintenance and post-maintenance reliability distributions. The resulting estimates therefore describe the observed alarm-related behaviour under the simplified model assumptions and should not be interpreted as reliability characteristics of an uninterrupted component lifetime.

The reliability function is given by:

$$R_i^{(b)}(t) = \begin{cases} 1, & t < 0 \\ exp[-\lambda_i^{(b)} t], & t \geq 0. \end{cases} \quad (32)$$

The parameter $\lambda_i^{(b)}$, $i$ = 1,2,3, $b$ = 1, 2, ..., 6, was estimated from empirical data (Table 5), namely

$$\lambda_i^{(b)} = \frac{1}{\frac{1}{n_i^{(b)}} \sum_{j=1}^{n_i^{(b)}} t_{i,j}^{(b)}}, \quad (33)$$

where $t_{i,j}^{(b)}, j = 1,2, \ldots, n_i^{(b)}$, are realisations of $T_i^{(b)}$, while $n_i^{(b)}$ is the number of these realisations, for $i$ = 1,2,3, $b$ = 1, 2, ..., 6, i.e., at states $hm_{\mathrm{L1}}$, $hm_{\mathrm{M1}}$, $hm_{\mathrm{H1}}$, $hm_{\mathrm{L2}}$, $hm_{\mathrm{M2}}$, $hm_{\mathrm{H2}}$:

$$\begin{aligned} &\lambda_i^{(hm_{L1})} \cong 1/23.852 \cong 0.042,\ \lambda_i^{(hm_{M1})} \cong 1/8.279 \cong 0.121,\ \lambda_i^{(hm_{H1})} \text{not estimated,} \\ &\lambda_i^{(hm_{L2})} \cong 1/5.022 \cong 0.199,\ \lambda_i^{(hm_{M2})} \cong 1/7.12 \cong 0.14,\ \lambda_i^{(hm_{H2})} \cong 1/6.2 \cong 0.161. \end{aligned} \quad (34)$$

No selected gyrocompass alarms were assigned to state $hm_{\mathrm{H1}}$ during its three-hour exposure. Therefore, the corresponding exponential rate parameter could not be estimated from the available alarm data. The contribution of this state to the unconditional reliability function was neglected because its estimated limiting probability was very small (approximately 0.00025, rounded to zero in Equation (29)), and the available alarm data did not permit a reliable state-specific rate parameter to be estimated. This does not imply that gyrocompass alarms or failures are impossible under these conditions.

The unconditional alarm-related reliability function of a single gyrocompass was approximated by a weighted mixture of exponential functions, using the limit transient hydro-meteorological state probabilities from Equations (12) and (29) and the conditional reliability functions defined in Equation (32):

$$\begin{aligned} R_i(t) &= 0.633 \cdot exp[-0.042t] + 0.254 \cdot exp[-0.121t] \\ &+ 0 + 0.019 \cdot exp[-0.199t] + 0.082 \cdot exp[-0.14t] \\ &+ 0.012 \cdot exp[-0.161t],\ t \geq 0. \end{aligned} \quad (35)$$

The plot of this function is presented in Figure 14.

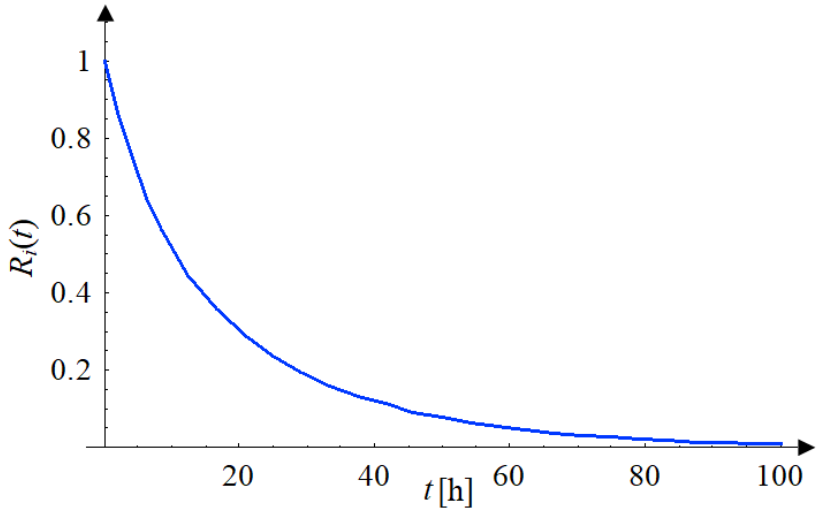



**Figure 14.** Reliability function of a single gyrocompass.

For the single gyrocompass reliability function, the calculated expected value, variance and standard deviation are

$$m = E(T_i) \cong 17.926 \text{ h}, D^2[T_i] \cong 441.285 \text{ h}^2, \ \sigma \cong 21.01 \text{ h}. \tag{36}$$

The reliability function of the three-gyrocompass system was calculated assuming a parallel configuration and statistically independent alarm-related events for the individual gyrocompasses. Under this simplifying assumption, the system TTF is $T = \max\{T_1, T_2, T_3\}$, which means that it remains operational as long as at least one gyrocompass remains available. The system reliability function is given by:

$$\begin{aligned} \boldsymbol{R}_S(t) &= 1 - \prod_{i=1}^{3} (1 - R_i(t)) \\ &= 1 - [1 - (0.633 \cdot \exp[-0.042t] + 0.254 \cdot \exp[-0.121t] + 0 \\ &+ 0.019 \cdot \exp[-0.199t] + 0.082 \cdot \exp[-0.14t] + 0.012 \cdot \exp[-0.161t])]^3. \end{aligned} \tag{37}$$

The function is presented in Figure 15.

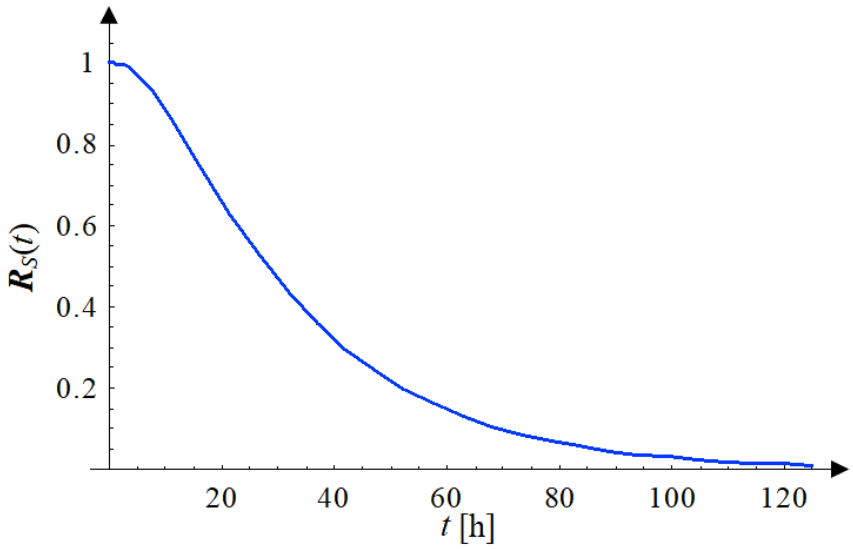



**Figure 15.** Reliability function of the system of three gyrocompasses.

The expected value, variance and standard deviation of the unconditional system TTF are then determined:

$$m = E[T] \approx 34.812 \text{ h}, D^2[T] \approx 684.802 \text{ h}^2, \ \sigma \approx 26.169 \text{ h}. \quad (38)$$

The failure intensity function of the system of gyrocompasses is shown in Figure 16.

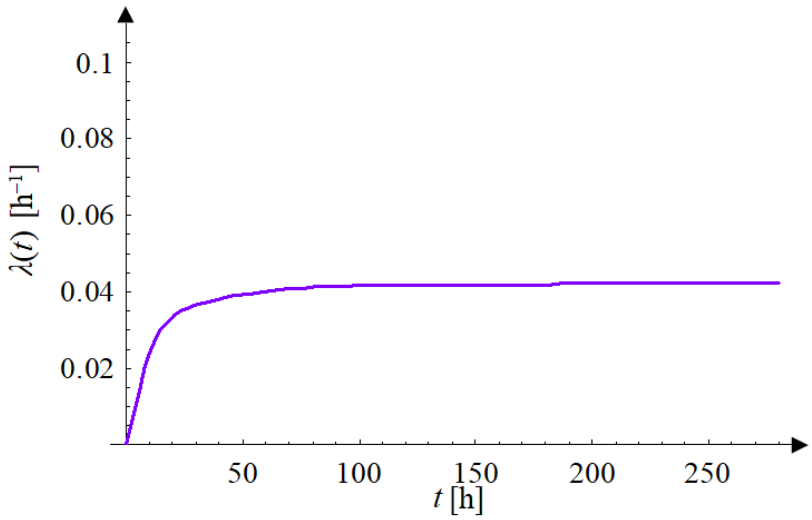



**Figure 16.** Failure intensity function of the system.

*5.7. Integration with the Risk Model*

The transition from gyrocompass failure to loss of reliable navigation information was modelled as a conditional process dependent on technical and human factors (see Section 4.3). The reliability results were integrated into the probabilistic risk model defined in Equation (18).The first probability term was calculated using the gyrocompass reliability function estimated from operational alarm data (Section 5.6), whereas the remaining conditional probabilities were evaluated using illustrative scenario parameters informed by maritime safety literature and industry reports, including DP incident reports published by IMCA [65], maritime casualty reports from the European Maritime Safety Agency [66,67], and oil spill statistics published by the International Tanker Owners Pollution Federation [68–71]. In practice, gyro failure does not immediately imply loss of position, as modern bridges incorporate redundancy, cross-checking procedures, and operator intervention. However, the literature consistently indicates that human and organisational factors can contribute significantly to navigation-related incidents [29,30,53,66,67]. Therefore, the conditional probability $P_{Lp|Gf}(t)$ was interpreted as a function of heading error magnitude, detection and response time, operator performance and workload.

The probability of an accident given loss of position was modelled using an encounter-based approach, linking risk to traffic density and exposure time. Empirical studies based on AIS data indicate that collision and grounding risk increases significantly with vessel density, proximity to navigational hazards and the duration of impaired situational awareness [7,8,12,51]. Typical values used in this study reflect moderate-to-high traffic scenarios, such as coastal areas. Under such conditions, even a temporary loss of accurate heading information can meaningfully increase accident probability [20].

Statistics published by the International Tanker Owners Pollution Federation [68–71] provide information on oil spills from tankers or fuel-carrying vessels, including their frequency, size and causes. The probability depends on impact energy, ship structural integrity, tank configuration, and accident type (collision vs. grounding) [49]. The occurrence of an oil spill following an accident also depends on accident type and vessel characteristics, as

demonstrated by probabilistic modelling of historical tanker accidents [49]. In this study, representative values consistent with historical observations were used to model $P_{S|A}(t)$, providing a literature-informed basis for the assumed oil spill consequence model.

To demonstrate the practical applicability of the proposed framework, a numerical evaluation was performed for a representative operating time horizon of $t = 10$ h. The analysis was carried out for both a single gyrocompass configuration and a system comprising three redundant gyrocompasses.

For the single gyrocompass, the probability of failure at $t = 10$ h was estimated as

$$P_{Gf}(10) = 1 - R_i(10) = 0.483137 \approx 0.48, \tag{39}$$

using Equation (35).

For the illustrative risk scenario, the following conditional probability parameters were adopted, with their selection informed by maritime safety literature and industry statistics. First, the conditional probability that a gyrocompass failure results in a loss of reliable navigation information at time $t$ was approximated using a multiplicative model reflecting the combined influence of heading error, response time, and human performance:

$$P_{Lp|Gf}(t) = f(\Delta\theta, t_r, H) = k_{Lp|Gf} \cdot f_1(\Delta\theta) \cdot f_2(t_r) \cdot f_3(H) = 0.2475 \approx 0.25, \tag{40}$$

where $f_1(\Delta\theta) = \Delta\theta/10$, $f_2(t_r) = t_r/10$, and $f_3(H) = 1 - H$. The denominators in $f_1$ and $f_2$ represent assumed reference values of 10° and 10 min, respectively, while $H$ is a dimensionless operator performance factor ranging from 0 to 1. The representative values are adopted as $\Delta\theta = 5°$, $t_r = 3$ min, $H = 0.7$, and the parameter $k_{Lp|Gf} \approx 5.5$ is introduced as a scaling factor accounting for the aggregate influence of unmodelled factors that are not explicitly represented in the simplified multiplicative structure [52,53]. The assumed heading error of 5° represents the downstream risk scenario and is distinct from the 2° DP alarm threshold used in the empirical analysis. An IMCA report concerning a DP Class 2 supply vessel documented heading excursions of approximately 3–5° during adverse weather conditions [65], providing an operational reference for the assumed 5° navigation-loss scenario. For the adopted values, the product of the three factors is 0.045, and the scaling coefficient of 5.5 gives $P_{Lp|Gf}(10) \approx 0.25$.

The probability of accident occurrence conditioned on loss of position was modelled using an encounter-based Equation (20):

$$P_{A|Lp}(t) = 1 - \exp(-D(t) \cdot T_e \cdot \beta(t)) = 0.0198 \approx 0.02, \tag{41}$$

where the parameter values were adopted for an illustrative moderate-risk scenario, with their selection informed by maritime traffic studies and AIS-based risk modelling literature [7,8,12,51]. Moderate traffic density was assumed to be $D = 10$ ships per 100 km$^2$, the exposure time (duration of navigation under degraded conditions) was $T_e = 1$ h, and the risk coefficient was$\beta = 0.002$ (100 km$^2$)/(ship · hour). These units ensure that the product $D \cdot T_e \cdot \beta$ is dimensionless. The adopted values represent a hypothetical moderate operating scenario corresponding to coastal or congested traffic conditions, rather than parameters calibrated directly from the vessel's accident records.

The probability that an accident results in an oil spill is evaluated using the scaling coefficient described in Section 4.3, the parameter values from Table 7 and structural reliability concepts:

$$\begin{aligned} P_{S|A}(t) &= k_{S|A} \cdot P\left(E_{impact} - E_{crit} > 0\right) = k_{S|A} \cdot P(Z > 0) \\ &= k_{S|A} \cdot P\left(\frac{Z - \mu_Z}{\sigma_Z} > 0.51\right) = k_{S|A} \cdot 0.304 \approx 0.10 \end{aligned} \tag{42}$$

**Table 7.** Parameters, interpretation and basis of selection for the probabilistic oil spill risk assessment.

| Parameter | Adopted Value | Meaning and Literature Basis |
|---|---|---|
| $t$ | 10 h | Evaluation time horizon for reliability and the resulting oil spill risk |
| $R_i(10)$ | 0.516863 | Single-gyrocompass reliability calculated from operational alarm data |
| $P_{Gf}(10)$ | 0.483137 | Probability of the modelled single gyrocompass event, calculated from $R_i(10)$ using operational alarm data |
| $\Delta\theta$ | 5° | Heading deviation selected for the navigation-loss scenario, with reference to documented DP heading excursions [65] |
| $t_r$ | 3 min | Response time selected for the scenario, considering operator intervention and human-related DP hazards [29,30] |
| $H$ | 0.70 | Dimensionless operator performance factor representing the influence of human response on navigation-information loss [29,53] |
| $k_{Lp\|Gf}$ | 5.5 | Scaling coefficient accounting for additional technical and operational factors in the simplified navigation-loss model |
| $P_{Lp\|Gf}(10)$ | 0.2475 | Conditional probability of navigation-information loss following the modelled gyrocompass event, calculated using Equation (40) |
| $D$ | 10 ships/100 km$^2$ | Traffic density adopted with reference to maritime traffic and collision-risk studies [7,8,12,51] |
| $T_e$ | 1 h | Exposure time under degraded navigation conditions |
| $\beta$ | 0.002 (100 km$^2$)/(ship·h) | Traffic-risk coefficient within the encounter-based accident model [7,8,12,51] |
| $P_{A\|Lp}(10)$ | 0.0198 | Conditional accident probability calculated using Equation (41) |
| $E_{impact}$ | $N(100,30^2)$ | Impact-related variable represented by a normal distribution within the structural reliability approach [54,55] |
| $E_{crit}$ | $N(120,25^2)$ | Structural resistance threshold represented by a normal distribution within an accidental-damage assessment, based on structural reliability and fragility concepts [54,55] |
| $k_{S\|A}$ | 0.33 | Scaling coefficient accounting for additional conditions affecting oil release after an accident [10,49,55,68–71] |

The impact-related variable $E_{impact}(t)$ was assumed to follow a normal distribution with mean 100 and standard deviation 30, while the corresponding structural resistance threshold $E_{crit}(t)$ was assumed to follow a normal distribution with mean 120 and standard deviation 25. Thus, assuming independence of these two variables, their difference $Z = E_{impact} - E_{crit}$ has a mean $\mu_Z = -20$ and a standard deviation $\sigma_Z = 39.05$, giving the reliability index $\mu_Z/\sigma_Z \approx -0.51$. Under the assumed distributions, $P(Z > 0) \approx 0.304$ indicates that approximately one-third of the considered accident scenarios involve impact energy exceeding the assumed structural resistance threshold. The adopted distributions were used within a simplified impact–resistance calculation, with reference to structural reliability methods [54] and accidental ship-damage assessment [55]. In the present case, the scaling coefficient $k_{S|A} \approx 0.33$ was adopted for the considered scenario. This parameter accounts for additional factors affecting the occurrence of an oil spill following an accident, which are not explicitly represented by the simplified impact–resistance model [10,47,49,68–71]. This value does not represent an empirically established proportion of accidents resulting in cargo release.

Combined with $P(Z > 0) \approx 0.304$, it gives an approximate conditional oil spill probability of $P_{S|A}(t) \approx 0.10$.

The selection of conditional risk parameters was informed by studies concerning maritime traffic and collision risk [7,8,12,51], DP hazards and human factors [29,30,53,65], probabilistic structural reliability [54,55], and oil spill occurrence and consequences [10,49,68–71]. The gyrocompass event probabilities were calculated separately using the operational alarm data.

Substituting the adopted parameter values from Equations (39)–(42) into the hierarchical risk model gives:

$$P_{oil\ spill}(10) \approx 0.0238\%. \tag{43}$$

The system-level probability of the modelled event was calculated using Equations (37) and (39), under the assumption of three independent gyrocompasses:

$$P_{S,Gf}(10) = 1 - \boldsymbol{R}_S(10) = 0.112775 \approx 0.113 \tag{44}$$

Applying the same conditional probabilities used for the single gyrocompass configuration and Equation (44), the estimated oil spill probability for the redundant system is:

$$P_{S,oilspill}(10) = 0.00555\% \approx 0.006\%. \tag{45}$$

Thus, under the independence assumption and for the selected parameter values, redundancy reduces the estimated oil spill probability by approximately 77% relative to the single gyrocompass configuration. The estimated overall risk also depends on the adopted conditional probabilities, including the probability of an accident following a loss of position and the probability of an oil spill given an accident. These conditional probabilities were assumed for the considered scenario rather than estimated from the vessel's operational data. Therefore, the results do not establish the relative importance of gyrocompass reliability and the downstream factors in actual maritime accidents.

The estimated oil spill probability in Equation (45) corresponds to approximately six cases per 100,000 hypothetical scenarios considered within the model. This value represents the probability of an oil spill resulting from a specific sequence of events: occurrence of the modelled system-level event in the three-gyrocompass configuration, subsequent loss of vessel position, accident occurrence and environmental release.

### *5.8. Sensitivity Analysis of the Risk Model*

A one-at-a-time (OAT) sensitivity analysis was conducted to examine the influence of selected parameters on the estimated oil spill probability for single-gyrocompass and three-gyrocompass configurations. The baseline parameter values were operator performance $H = 0.70$, response time $t_r = 3$ min, traffic risk coefficient $\beta = 0.002$, spill scaling factor $k_{S|A} = 0.33$, and the probability of failure $P_{Gf}(10) = 0.483137$. $H$ was varied by $\pm 0.10$, while the other parameters were varied by $\pm 20\%$ of their baseline values. Each parameter was changed individually, with the remaining parameters held at their baseline values.

The calculations were performed using the probability expressions defined in Equations (35) and (40)–(42), without intermediate rounding. For the baseline scenario, $R_i(10) = 0.516863$, the failure probability of the three-gyrocompass system was $P_{S,Gf}(10) = 0.112775$, and the estimated oil spill probabilities were $P_{oil\ spill}(10) = 0.023775\%$ and $P_{S,oil\ spill}(10) = 0.005549\%$. The selected ranges were used to illustrate the response of the risk model to parameter variation and do not represent empirically established confidence intervals. The results are presented in Table 8.

**Table 8.** Results of the sensitivity analysis.

| Parameter | Base Value | Value | Single Gyro [%] | Three Gyros [%] | Risk Reduction [%] |
|---|---|---|---|---|---|
| Baseline | – | – | 0.02377 | 0.00555 | 76.66 |
| $H$ | 0.7 | 0.60 | 0.03170 | 0.00740 | 76.66 |
| | | 0.80 | 0.01585 | 0.00370 | 76.66 |
| $t_r$ [min] | 3 [min] | 2.4 | 0.01902 | 0.00444 | 76.66 |
| | | 3.6 | 0.02853 | 0.00666 | 76.66 |
| $\beta$ | 0.002 | 0.0016 | 0.01906 | 0.00445 | 76.66 |
| | | 0.0024 | 0.02847 | 0.00665 | 76.66 |
| $k_{S\|A}$ | 0.33 | 0.264 | 0.01902 | 0.00444 | 76.66 |
| | | 0.396 | 0.02853 | 0.00666 | 76.66 |
| $P_{Gf}(10)$ | 0.483137 | 0.38651 | 0.01902 | 0.00284 | 85.06 |
| | | 0.57976 | 0.02853 | 0.00959 | 66.39 |

The results show that changes in operator performance, response time, traffic risk coefficient and spill scaling factor affect the absolute oil spill probability in both configurations. However, the relative risk reduction associated with redundancy remains unchanged at approximately 76.7% when the same conditional probabilities are applied to both configurations:

$$risk_{reduction} = 1 - \frac{(P_{Gf}(10))^3 \cdot P_{Lp|Gf}(10) \cdot P_{A|Lp}(10) \cdot P_{S|A}(10)}{P_{Gf}(10) \cdot P_{Lp|Gf}(10) \cdot P_{A|Lp}(10) \cdot P_{S|A}(10)} = 1 - (P_{Gf}(10))^2 \approx 76.66\% \quad (46)$$

In contrast, varying the single-gyrocompass failure probability by ±20% changes the estimated relative risk reduction from approximately 66% to 85%. Within the adopted model, the relative benefit of redundancy is determined by the single-gyrocompass failure probability when the downstream conditional probabilities are identical for both configurations. The sensitivity results therefore quantify how uncertainty in this probability affects the estimated risk reduction.

These findings demonstrate the dependence of the numerical risk estimates on the adopted model parameters. The results remain conditional on the assumption of independent gyrocompass failures. Common-cause failures are not represented in the present sensitivity analysis and could reduce the estimated benefit of redundancy.

## 6. Discussion

The hydro-meteorological conditions recorded in the deck logs of *Troms Capella* varied with the vessel's location over the study period.

The chart in Figure 17 presents the duration of individual hydro-meteorological states over the entire study period. State $hm_{\mathrm{L1}}$clearly dominates, accounting for nearly two-thirds of the total observation time. This state corresponds to conditions where wave height does not exceed 3m and wind speed remains below Beaufort force 7, representing relatively mild operating conditions. It also includes the periods when the vessel was in port. The second most frequent state in the analysed dataset is $hm_{\mathrm{M1}}$, which is typical in the North Sea conditions. Notably, state $hm_{\mathrm{H1}}$ occurred only once, lasted 3 hand accounted for a negligible proportion of the total observation time. This limited exposure does not allow reliable conclusions to be drawn about the frequency of such conditions or the associated gyrocompass alarm occurrence.

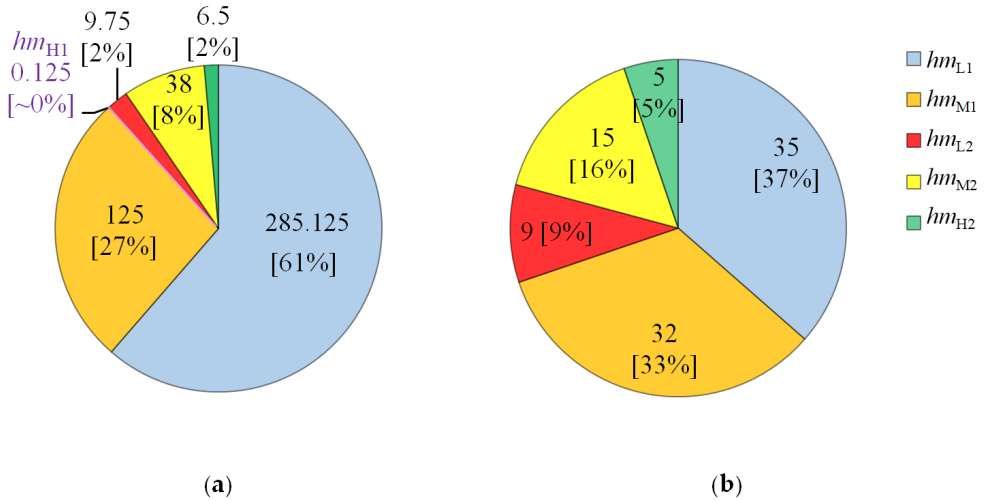



**Figure 17.** Summary of the duration of hydro-meteorological states: (**a**) duration in days; (**b**) distribution of selected alarm records across states.

The alarm counts were compared with the exposure duration of each hydro-meteorological state to account for the substantial differences in the time spent in individual states (Figure 17). The number of selected alarm records per 100 days of exposure is given in Table 9. The exposure-normalised results show that $hm_{L2}$ had the highest observed alarm frequency, with 92.31 selected alarm records per 100 days of exposure, followed by $hm_{H2}$ (76.92) and $hm_{M2}$ (39.47). A similar pattern was observed for alarm weights per day, with the highest value recorded in $hm_{L2}$ (16.51), followed by $hm_{H2}$ (10.00) and $hm_{M2}$ (4.34). These findings indicate differences in recorded gyrocompass alarm occurrence between hydro-meteorological states. However, the results should be interpreted with caution because of the relatively short exposure duration in $hm_{L2}$ (9.75 days) and $hm_{H2}$ (6.5 days), the event-selection procedure, and the fact that heading-deviation alarms do not necessarily represent confirmed physical failures. Furthermore, $hm_{H1}$ was observed for only 0.125 days (3 h), with no selected alarms assigned to this state, which is insufficient to draw reliable conclusions about its associated alarm frequency.

**Table 9.** Summary of hydro-meteorological state data and associated alarm records.

| State | Exposure [Days] | Alarm Records | Percentage | Records per 100 Days | Sum of Weights | Percentage | Weights per Day |
|---|---|---|---|---|---|---|---|
| $hm_{L1}$ | 285.125 | 35 | 36.5% | 12.28 | 400 | 35% | 1.4 |
| $hm_{M1}$ | 125 | 32 | 33.3% | 25.6 | 357 | 31% | 2.86 |
| $hm_{H1}$ | 0.125 | 0 | 0% | 0 | 0 | 0% | 0 |
| $hm_{L2}$ | 9.75 | 9 | 9.4% | 92.31 | 161 | 14% | 16.51 |
| $hm_{M2}$ | 38 | 15 | 15.6% | 39.47 | 165 | 14% | 4.34 |
| $hm_{H2}$ | 6.5 | 5 | 5.2% | 76.92 | 65 | 6% | 10 |
| Sum | 464.5 ≈ 465 | 96 | 100% | – | 1148 | 100% | – |

It should be noted that wave height values do not strictly correspond to Beaufort scale intervals, as the dataset includes port stays where wave height was not recorded and was assumed to be zero. Additionally, wave height measurements are subject to uncertainty due to their visual estimation by the officer on watch. In contrast, wind speed measurements represent 10 min averages obtained from high-precision ultrasonic anemometers installed on the vessel's mast (marked with red circles in Figure 6).

The estimated reliability results also demonstrate the benefit of the three-gyrocompass configuration. Even if one gyrocompass becomes unavailable, the redundant system can

continue to provide heading information. The comparison of the estimated mean time to the modelled alarm-related event for a single gyrocompass (~17.9 h) and for the three-gyrocompass system (~34.8 h) indicates that redundancy substantially extends the expected alarm-free operating period under the adopted model assumptions. A deviation of 2° between gyrocompass indications does not, by itself, demonstrate a loss of navigational capability. Nevertheless, such deviations require appropriate attention from the DP operator.

Despite technical measures intended to reduce wave-induced deviations, the observed alarm frequencies varied between hydro-meteorological states (Figure 18). The highest alarm weight per day was recorded in $hm_{L2}$, followed by $hm_{H2}$ and $hm_{M2}$. This indicates that alarm occurrence was not uniformly associated with increasing wind speed and wave height. The observed differences may also reflect operational and equipment-related factors. Furthermore, the installation location of gyrocompasses may influence their response to vessel motion, as positioning them closer to the vessel's centre of roll could reduce the accelerations affecting their operation, which may contribute to wave-induced deviations [32,61].

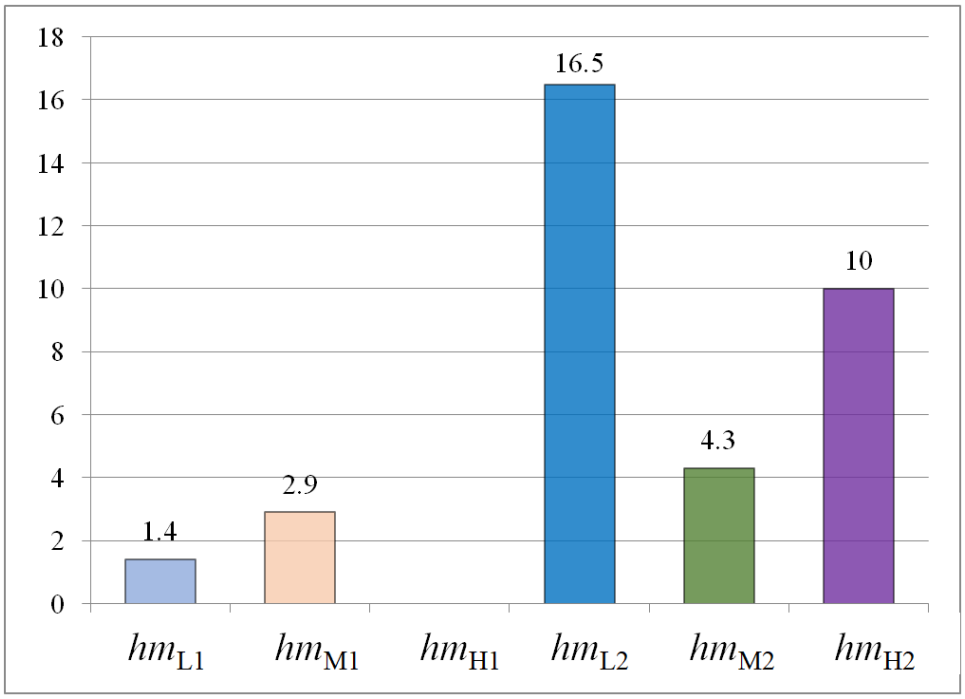



**Figure 18.** Alarm weights per day.

Comparison of the maintenance records in Appendix B with the alarm data indicates that the gyro sphere replacements were followed by a substantial reduction in recorded heading-deviation alarms. The gyro sphere in compass no. 1 was replaced on 29.11.2019, and over the following six months only one alarm was recorded, occurring one day after the repair. Similarly, after replacing the gyro sphere in compass no. 2 on 27.02.2020, only one alarm occurred during the subsequent three months, also one day after the repair. The reduction in recorded alarms following gyro sphere replacement suggests that maintenance interventions may have influenced subsequent operational behaviour. However, the available observations do not allow the effect of maintenance on the failure intensity to be quantified separately. This represents a limitation of the adopted exponential reliability model. Future research could consider a more realistic model, e.g., one involving a Weibull distribution (ageing effects) or renewal process modelling.

While the semi-Markov model captures the stochastic evolution of hydro-meteorological states, the influence of these states on the downstream conditional probabilities represents a potential extension of the proposed approach. More severe conditions may increase heading instability and operator workload, potentially reducing effective operator performance ($H$) and increasing response time ($t_r$). These state-dependent relationships were not estimated directly from the available data. Their inclusion would require additional observations and a corresponding extension of the probabilistic risk model.

The results of the integrated reliability–risk assessment demonstrate that gyrocompass redundancy can substantially reduce the estimated probability of an oil spill within the considered scenario. For the adopted time horizon and parameter values, the three-gyrocompass configuration reduces the estimated oil spill probability by approximately 77% compared with a single gyrocompass. This reduction results from the lower probability of system-level failure under the assumption of independent gyrocompass failures.

The final risk estimate also depends on the conditional probabilities associated with loss of reliable navigation information, accident occurrence and oil release. These probabilities were adopted for the analysed scenario and were not estimated directly from the vessel's operational data. Consequently, the quantitative results should be interpreted in the context of the assumptions underlying the probabilistic risk model. In practical applications, the benefits of sensor redundancy should therefore be considered alongside operator response, navigation procedures and other measures intended to prevent the escalation of equipment-related disturbances into accidents.

The sensitivity analysis presented in Section 5.8 demonstrates that the estimated oil spill probability depends on the adopted conditional parameters, whereas the relative benefit of redundancy remains constant when these parameters are applied identically to both configurations. However, changes in the single-gyrocompass failure probability affect the estimated risk reduction. Further research should therefore investigate the uncertainty associated with the empirical reliability estimates and the potential influence of common-cause failures on the effectiveness of redundancy.

The assumption of independent gyrocompass failures represents a limitation of the adopted parallel reliability model. Although the three gyrocompasses provide redundant heading measurements, their operation may be affected by common disturbances, including severe vessel motions, power supply disturbances, environmental conditions, installation-related factors and maintenance procedures. Such factors could cause simultaneous degradation of multiple gyrocompasses and reduce the reliability benefit predicted under the independence assumption. Furthermore, correlated heading errors may be difficult to identify through comparison with the median of the available measurements. The estimated risk reduction of approximately 77% should therefore be interpreted as a result obtained under the assumed independent-failure model. A more comprehensive assessment would require information on correlated failures and the introduction of common-cause failure mechanisms into the reliability model.

Although the empirical analysis was conducted using data from a single PSV, the *Troms Capella*, the proposed methodology is not limited to this vessel or its operating area. The developed framework can be applied to other vessels operating under different hydro-meteorological conditions, provided that the relevant operational and environmental data are available. The semi-Markov model, reliability assessment and probabilistic risk framework retain their general structure, while the hydro-meteorological state probabilities, alarm occurrence characteristics and reliability parameters are estimated using data specific to the analysed vessel. Consequently, the numerical results presented in this study describe the investigated case, whereas the proposed methodology provides a general framework

for assessing navigation system reliability and its contribution to environmental risk across different maritime operating conditions.

Future research may also include a scenario-based analysis in which the model is evaluated under distinct operational conditions. Representative scenarios may include calm offshore operations corresponding to state $hm_{\mathrm{L1}}$, moderate hydro-meteorological conditions represented by states $hm_{\mathrm{M1}}$ and $hm_{\mathrm{M2}}$, and severe weather conditions associated with state $hm_{\mathrm{H2}}$. Comparing the resulting $P_{oil\ spill}(t)$ across these scenarios would provide insight into how environmental variability affects the propagation of risk through the system. In addition, the modelling framework could be significantly strengthened by introducing a state-dependent formulation. In particular, the conditional probabilities $P_{Lp|Gf}(t)$ and $P_{A|Lp}(t)$ could be extended to explicitly depend on the hydro-meteorological states of the process $HM(t)$. This extension would directly integrate the semi-Markov environmental model with the reliability and risk components, leading to a fully coupled state-dependent risk representation. Finally, future research could extend the present probability-chain model by introducing a Monte Carlo simulation approach. By simulating gyrocompass alarm-related events, environmental state transitions and accident occurrences, the model could be used to analyse the distribution of simulated outcomes. Incorporating uncertainty in the input parameters would additionally allow uncertainty intervals to be estimated for the resulting oil spill probability.

## 7. Conclusions

The study identified differences in gyrocompass alarm occurrence across hydro-meteorological states based on operational data collected from a Platform Supply Vessel. The applied methodology, based on discretisation of environmental data and semi-Markov modelling, enabled the identification of relationships between environmental states and system reliability. Mild conditions (state $hm_{\mathrm{L1}}$) dominated the observation period, whereas the highest exposure-normalised alarm frequency was recorded in state$hm_{\mathrm{L2}}$, followed by $hm_{\mathrm{H2}}$ and $hm_{\mathrm{M2}}$. These findings suggest an association between environmental conditions and alarm occurrence, although the limited exposure in some states prevents more general conclusions.

Under the adopted independence assumption, the redundant configuration of three gyrocompasses substantially improved the modelled alarm-related reliability, with the estimated mean time to the modelled event approximately twice that of a single unit. Maintenance actions, such as gyro sphere replacements, were followed by a substantial reduction in recorded alarms, although the available data do not establish a direct causal relationship. The observed differences in alarm occurrence between hydro-meteorological states do not provide direct evidence of accelerated wear of gyrocompass components. Therefore, further studies incorporating technical condition assessments and maintenance records would be required to investigate the potential effects of prolonged exposure to harsh hydro-meteorological conditions on component wear.

The study also integrates the semi-Markov description of hydro-meteorological conditions with alarm-based gyrocompass reliability estimates and an illustrative probabilistic environmental risk framework using parameters selected with reference to maritime safety literature. The unconditional gyrocompass reliability function was represented as a weighted mixture of exponential functions associated with the individual hydro-meteorological states. The subsequent risk assessment incorporated conditional probabilities adopted for a representative operational scenario rather than estimated directly from the vessel's accident records. For the selected time horizon, the three-gyrocompass configuration produced a lower estimated oil spill probability than the single-gyrocompass configuration. This

result is conditional on the adopted parameter values and the assumption of independent gyrocompass failures.

A sensitivity analysis was conducted to evaluate the influence of selected model parameters on the estimated oil spill probabilities. The study also highlighted important sources of uncertainty, including the limited operational dataset, the simplified reliability assumptions, the use of heading-deviation alarms as indicators of performance degradation, and the adopted conditional risk parameters. These limitations should be considered when interpreting the numerical results and applying the methodology to other operational cases.

Finally, the proposed approach provides a useful basis for integrating navigation system reliability into broader risk assessment frameworks, including those related to offshore operational safety and environmental risk. The study also identified potential methodological extensions, including more extensive sensitivity and uncertainty analyses of key parameters, scenario-based evaluation of operational conditions, state-dependent probability coupling, and Monte Carlo simulation of the full risk propagation chain. These extensions provide directions for future development of the proposed framework.

**Funding:** The APC was funded by Gdynia Maritime University, Faculty of Computer Science (Research Project Manager: Ewa Dąbrowska; Research project topic: Modeling and simulation of the consequences of maritime accidents, including oil spills; Research project number: WI/2026/PI/03).

**Data Availability Statement:** The original contributions presented in this study are included in the article and supplementary material (Appendices A and B). Further inquiries can be directed to the corresponding author, upon reasonable request.

**Acknowledgments:** The paper presents the results obtained as part of statutory research activities and was supported by Gdynia Maritime University, Faculty of Computer Science (WI/2026/PI/03, WI/2026/PZ/03).

**Conflicts of Interest:** The author declares no conflicts of interest. The funders had no role in the design of the study; in the collection, analyses, or interpretation of data; in the writing of the manuscript; or in the decision to publish the results.

## Appendix A. Hydro-Meteorological Process Data

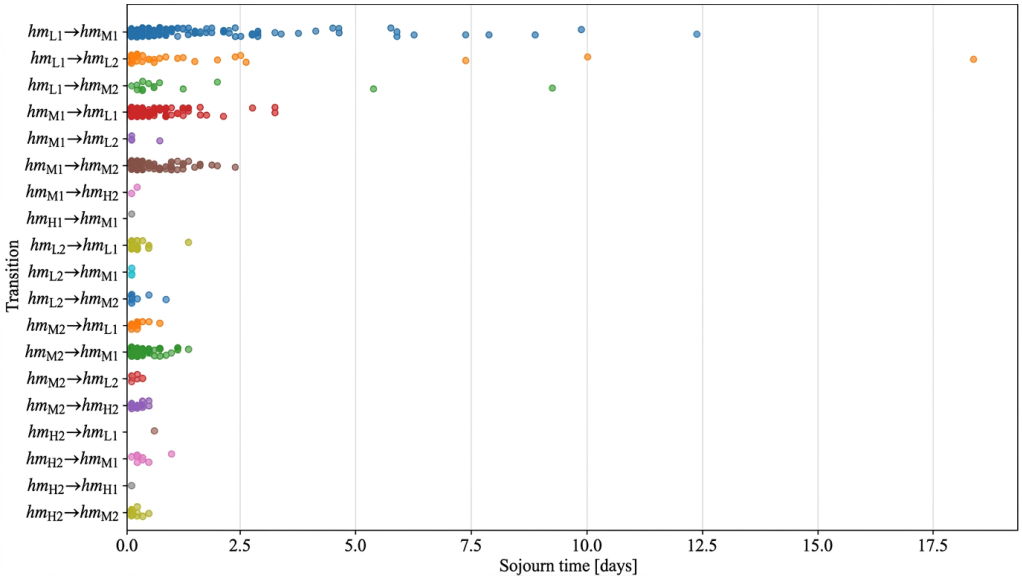



**Figure A1.** Conditional sojourn times for individual hydro-meteorological state transitions.

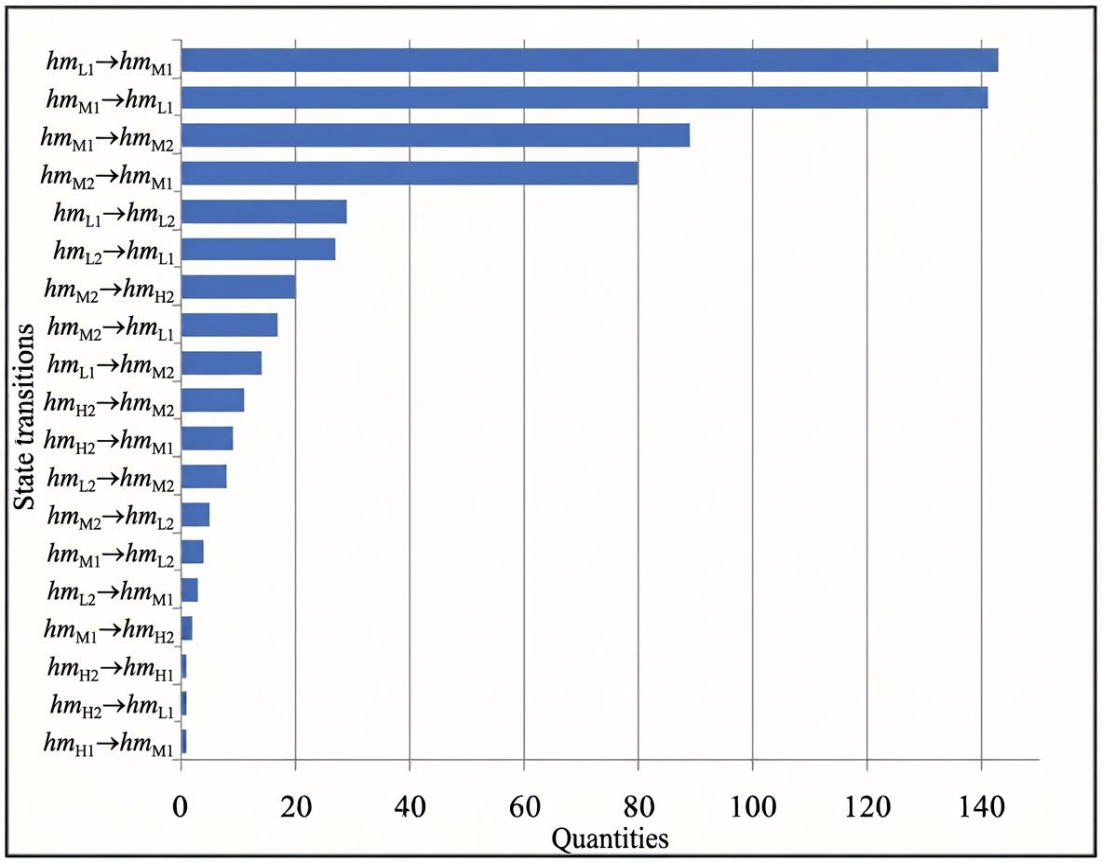



**Figure A2.** Number of transition realisations.

## Appendix B. Gyrocompass Reliability Data

The following service records summarise gyrocompass maintenance interventions and operating observations [62–64]. The 167 low compass-fluid-level alarms recorded for gyrocompass no. 2 concern a different alarm type from the heading-deviation events used in the reliability analysis.

- Service dated 24.10.2019:
  a. Gyrocompass no. 1: Inspection was postponed until the next port call;
  b. Gyrocompasses nos. 2 and 3: Routine maintenance was performed, and the pump motor was replaced;
  c. Gyrocompass no. 2: A total of 167 low compass-fluid-level alarms were recorded prior to maintenance.
- Service dated 05.11.2019:
  a. Gyrocompass no. 1: Maintenance was performed;
  b. Gyrocompass no. 2: A tendency to generate DP system alarms related to heading deviations from the median of the three gyrocompasses was observed; continuous monitoring was recommended.
  c. Gyrocompass no. 3: The alignment was adjusted.
- Service dated 29.11.2019:
  a. Gyrocompass no. 1: The gyro sphere was replaced.
- Service dated 27.02.2020:
  a. Gyrocompass no. 2: The gyro sphere was replaced.

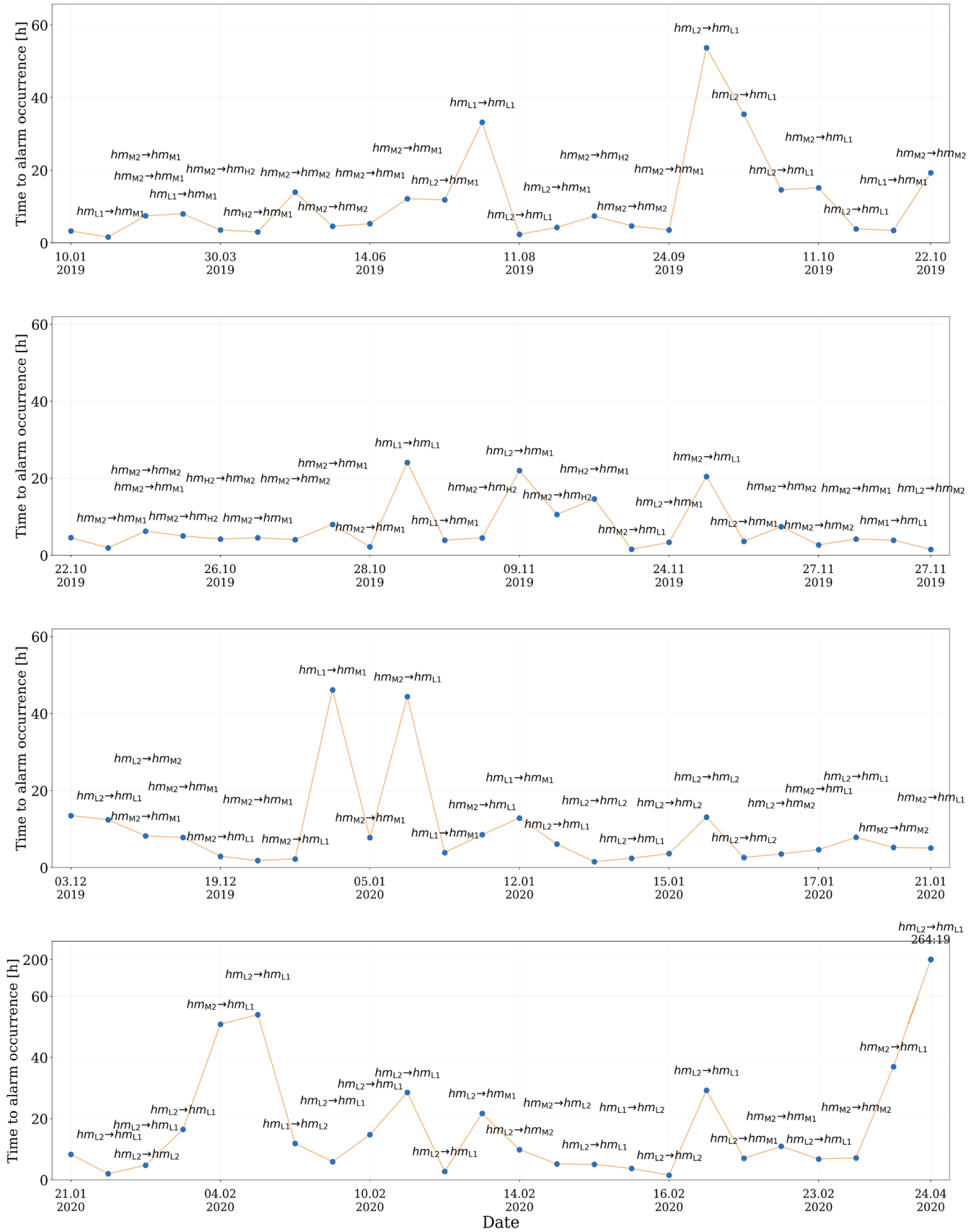



**Figure A3.** Selected alarm events and numerical times to alarm occurrence [h] (raw data).

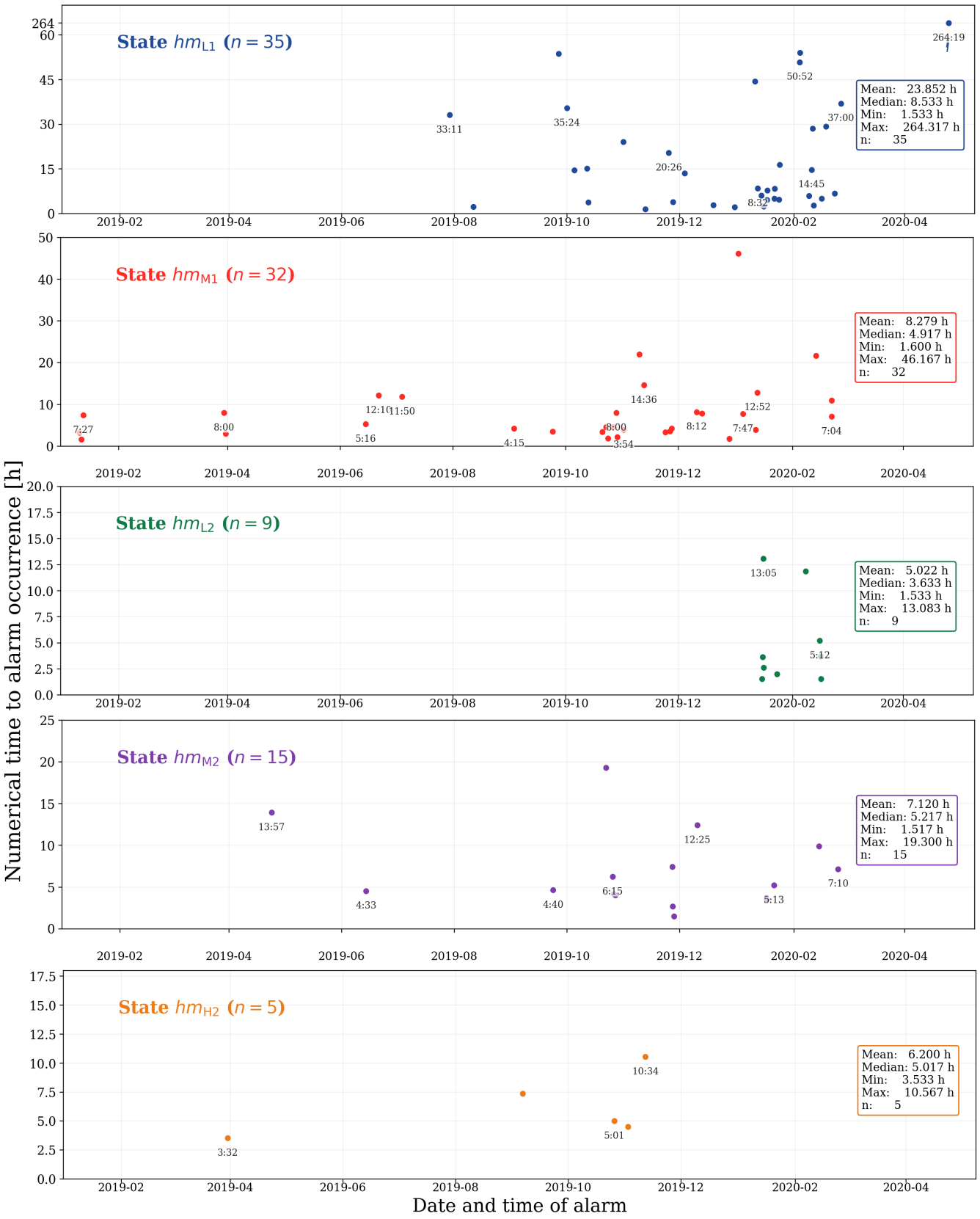



**Figure A4.** System alarms (raw data) during hydro-meteorological states.

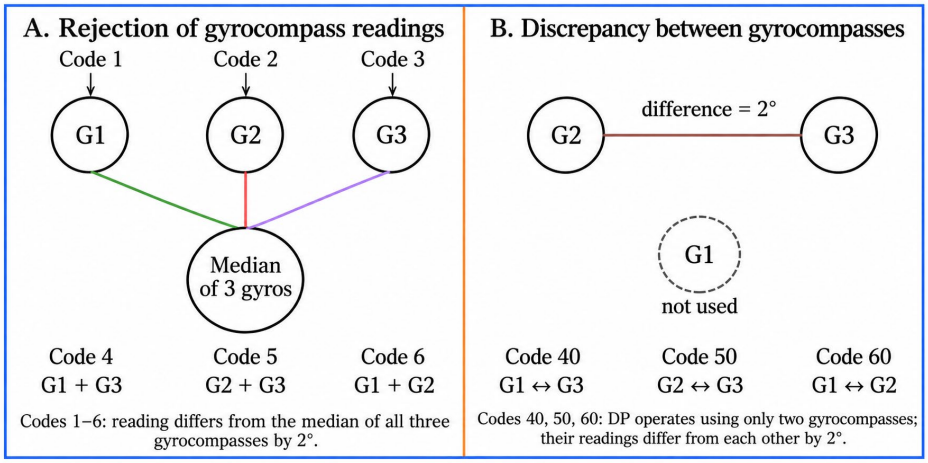



**Figure A5.** Gyro codes recorded—classification.

## References

1. Aziz, A.; Ahmed, S.; Khan, F.; Stack, C.; Lind, A. Operational risk assessment model for marine vessels. *Reliab. Eng. Syst. Saf.* **2019**, *185*, 348–361. [CrossRef]
2. Hu, S.P.; Fang, Q.; Xia, H.B.; Xi, Y.T. Formal safety assessment based on relative risks model in ship navigation. *Reliab. Eng. Syst. Saf.* **2007**, *92*, 369–377. [CrossRef]
3. Ozbas, B. Safety risk analysis of maritime transportation: Review of literature. *Transp. Res. Rec.* **2013**, *2326*, 32–38. [CrossRef]
4. International Marine Contractors Association (IMCA). *Guidelines for the Design and Operation of Dynamically Positioned Vessels*; M103 Rev. 2; International Marine Contractors Association (IMCA): London, UK, 2016.
5. International Maritime Organization (IMO). *Guidelines for Vessels with Dynamic Positioning Systems*; MSC/Circ. 645; International Maritime Organization (IMO): London, UK, 1994.
6. Adland, R.; Jia, H.Y.; Lode, T.; Skontorp, J. The value of meteorological data in marine risk assessment. *Reliab. Eng. Syst. Saf.* **2021**, *209*, 107480. [CrossRef]
7. Goerlandt, F.; Montewka, J. Maritime transportation risk analysis: Review and analysis in light of some foundational issues. *Reliab. Eng. Syst. Saf.* **2015**, *138*, 115–134. [CrossRef]
8. Antao, P.; Sun, S.; Teixeira, A.P.; Guedes Soares, C. Quantitative assessment of ship collision risk influencing factors from worldwide accident and fleet data. *Reliab. Eng. Syst. Saf.* **2023**, *234*, 109166. [CrossRef]
9. Bogalecka, M.; Dąbrowska, E. Monte Carlo simulation approach to shipping accidents consequences assessment. *Water* **2023**, *15*, 1824. [CrossRef]
10. Goerlandt, F.; Montewka, J. Probabilistic model for accidental cargo oil outflow from product tankers in a ship-ship collision. *Mar. Pollut. Bull.* **2014**, *79*, 130–144. [CrossRef] [PubMed]
11. Aven, T. Selective critique of risk assessments with recommendations for improving methodology and practice. *Reliab. Eng. Syst. Saf.* **2011**, *96*, 509–514. [CrossRef]
12. Du, L.; Goerlandt, F.; Kujala, P. Review and analysis of methods for assessing maritime waterway risk based on non-accident critical events detected from AIS data. *Reliab. Eng. Syst. Saf.* **2020**, *200*, 106933. [CrossRef]
13. Kołowrocki, K.; Kuligowska, E.; Soszyńska-Budny, J.; Torbicki, M. An approach to safety prediction of critical infrastructure impacted by climate-weather change process. In *Proceedings of the International Conference on Information and Digital Technologies 2017 (IDT 2017), 5–7 July 2017*; IEEE: New York, NY, USA, 2017; pp. 183–186. [CrossRef]
14. Kołowrocki, K.; Kuligowska, E.; Soszyńska-Budny, J. On multistate technical system operation process influence on its reliability. In *Safety and Reliability: Methodology and Applications*; Taylor & Francis Group: London, UK, 2015; pp. 2099–2106.
15. Chen, H.; Moan, T.; Verhoeven, H. Effect of DGPS failures on dynamic positioning of ships. *Accid. Anal. Prev.* **2009**, *41*, 1164–1171. [CrossRef] [PubMed]
16. Jaskólski, K. Methodology for Verifying the Indication Correctness of a Vessel Compass Based on the Spectral Analysis of Heading Errors and Reliability Theory. *Sensors* **2022**, *22*, 2530. [CrossRef] [PubMed]
17. Vedachalam, V.; Ramadass, G.A. Reliability assessment of multi-megawatt capacity offshore dynamic positioning systems. *Appl. Ocean. Res.* **2017**, *63*, 251–261. [CrossRef]
18. Wang, F.; Bai, Y.; Wang, J. Systematic reliability analysis of dynamic positioning control system for deepwater drilling rig. *Ships Offshore Struct.* **2021**, *16*, 1114–1124. [CrossRef]

19. Wang, F.; Zhao, L.; Bai, Y. Survey on reliability analysis of dynamic positioning systems. *Ships Offshore Struct.* **2024**, *19*, 999–1009. [CrossRef]
20. Bogalecka, M. *Consequences of Maritime Critical Infrastructure Accidents: Environmental Impacts Modeling-Identification-Prediction-Optimization-Mitigation*; Elsevier: Amsterdam, The Netherlands, 2020.
21. International Marine Contractors Association (IMCA). *Loss of Gyro Input Causes Loss of Position*; DP Incident Report; IMCA: London, UK, 2020.
22. Sanchez-Varela, Z.; Boullosa-Falces, D.; Larrabe Barrena, J.L.; Gomez-Solaeche, M.A. Prediction of Loss of Position during Dynamic Positioning Drilling operations Using Binary Logistic Regression Modeling. *J. Mar. Sci. Eng.* **2021**, *9*, 139. [CrossRef]
23. International Marine Contractors Association (IMCA). *Loss of DP Position Caused by Incorrect Gyro Heading*; Safety Flash 09/08; IMCA: London, UK, 2008.
24. Transportation Safety Board of Canada. Marine Investigation Report M14C0106. 2015. Available online: https://tsb.gc.ca/eng/rapports-reports/marine/2014/m14c0106/m14c0106.html (accessed on 13 March 2025).
25. Transportation Safety Board of Canada. *Marine Investigation Report M95L0189*; Transportation Safety Board of Canada: Gatineau, QC, Canada, 1996.
26. Jaskólski, K.; Czapliński, W.; Tomczak, A. Spectral Analysis of Compass Errors Based on Fast Fourier Transform and Reduction Absolute Errors Using a Pass-Band Finite Impulse Response Filter. *Pol. Marit. Res.* **2024**, *31*, 109–120. [CrossRef]
27. Dhyani, A.; van der El, K.; Negenborn, R.R.; Reppa, V. Multiple Sensor Fault Diagnosis for Safe Navigation of Autonomous Surface Vessels. *Control Eng. Pract.* **2026**, *168*, 106673. [CrossRef]
28. Jahani, S.; Zhou, S.; Veeramani, D. Stochastic prognostics under multiple time-varying environmental factors. *Reliab. Eng. Syst. Saf.* **2021**, *215*, 107877. [CrossRef]
29. Sanchez-Varela, Z.; Boullosa-Falces, D.; Skoko, I.; Boko, Z. Analysis of Human-Related Incidents during Dynamic Positioning Operations. *J. Mar. Sci. Eng.* **2024**, *12*, 907. [CrossRef]
30. Ataş, M.; Demirel, H. Ensuring Safety and Reliability in Offshore Operations: A Fuzzy DEMATEL Study on Dynamic Positioning System Hazards. *Ocean Eng.* **2025**, *337*, 121884. [CrossRef]
31. Burger, W. *Marine Gyro-Compasses and Automatic Pilots: A Handbook for Merchant Navy Officers*; The Macmillan Company: New York, NY, USA, 1963.
32. Krajczyński, E. *Urządzenia Elektronawigacyjne (eng. Electronavigation Devices)*; Wyższa Szkoła Morska w Gdyni: Gdynia, Poland, 2001.
33. Kołowrocki, K.; Dąbrowska, E. Hydro-meteorological change process impact on oil spill domain movement at sea. In *Theory and Applications of Dependable Computer Systems*; Proceedings of the Fifteenth International Conference on Dependability of Computer Systems, DepCos-Relcomex; Springer: Berlin/Heidelberg, Germany, 2020; pp. 165–175. [CrossRef]
34. Dąbrowska, E. Oil discharge trajectory simulation at selected Baltic Sea waterway under variability of hydro-meteorological conditions. *Water* **2023**, *15*, e1957. [CrossRef]
35. Jain, I.; Gautam, A.; Selvamuthu, D.; Xie, M. Semi-Markov modeling approach for the reliability analysis of a multiple high altitude platform station system. *Reliab. Eng. Syst. Saf.* **2026**, *265*, e111450. [CrossRef]
36. Kołowrocki, K.; Kuligowska, E. Operation and climate-weather change impact on maritime ferry safety. In *Safety and Reliability—Safe Societies in a Changing World*; Taylor & Francis Group: London, UK, 2018; pp. 849–858. [CrossRef]
37. Limnios, N.; Oprisan, G. *Semi-Markov Processes and Reliability*; Birkhauser: Boston, MA, USA, 2001. [CrossRef]
38. Xue, J. On multi-state system analysis. *IEEE Trans. Reliab.* **1985**, *34*, 329–337. [CrossRef]
39. Woch, M. Reliability Analysis of the PZL-130 Orlik TC-II Aircraft Structural Component Under Real Operating Conditions. *Eksploat. I Niezawodn.-Maint. Reliab.* **2017**, *19*, 287–295. [CrossRef]
40. Ware, A.; Collette, M. Statistical Reliability Analysis of Marine Systems with Varied Levels of Redundancy. In Proceedings of the International Marine Design Conference (IMDC 2024), Amsterdam, The Netherlands, 2–6 June 2024. [CrossRef]
41. Kołowrocki, K.; Kuligowska, E.; Soszyńska-Budny, J.; Torbicki, M. Safety and risk prediction of port oil piping transportation system impacted by climate-weather change process. In *Proceedings of the International Conference on Information and Digital Technologies 2017 (IDT 2017), 5–7 July 2017*; IEEE: New York, NY, USA, 2017; pp. 173–177. [CrossRef]
42. Pietrucha-Urbanik, K. Assessing the costs of losses incurred as a result of failure. In *Dependability Engineering and Complex Systems*; Zamojski, W., Mazurkiewicz, J., Sugier, J., Walkowiak, T., Kacprzyk, J., Eds.; Springer: Cham, Switzerland, 2016; Volume 470, pp. 355–362. [CrossRef]
43. Zhou, D.; Sun, C.P.; Du, Y.-M.; Guan, X. Degradation and reliability of multi-function systems using the hazard rate matrix and Markovian approximation. *Reliab. Eng. Syst. Saf.* **2022**, *218*, e108166. [CrossRef]
44. Bogalecka, M.; Kołowrocki, K. Prediction of critical infrastructure accident losses of chemical releases impacted by climate-weather change. In *Proceedings of the 2018 IEEE International Conference on Industrial Engineering and Engineering Management (IEEM), 16–19 December 2018*; IEEE: New York, NY, USA, 2018; pp. 788–792. [CrossRef]

45. Bogalecka, M.; Magryta-Mut, B.; Torbicki, M. Climate Resilient Maritime Transport: Probabilistic Modeling of Operational Costs Under Increasing Weather Variability in the Baltic Sea. *Sustainability* **2026**, *18*, e1592. [CrossRef]
46. Kołowrocki, K.; Kuligowska, E.; Soszyńska-Budny, J.; Torbicki, M. Simplified impact model of critical infrastructure safety related to climate-weather change process. In *Proceedings of the International Conference on Information and Digital Technologies 2017 (IDT), 5–7 July 2017*; IEEE: New York, NY, USA, 2017; pp. 187–190. [CrossRef]
47. Lehikoinen, A.; Hänninen, M.; Storgård, J.; Luoma, E.; Mäntyniemi, S.; Kuikka, S. A Bayesian Network for Assessing the Collision Induced Risk of an Oil Accident in the Gulf of Finland. *Environ. Sci. Technol.* **2015**, *49*, 5301–5309. [CrossRef] [PubMed]
48. Dąbrowska, E. Probabilistic solution for reducing oil spill contamination risk on port critical infrastructure safety. *Reliab. Eng. Syst. Saf.* **2026**, *268*, 111961. [CrossRef]
49. Sevgili, C.; Fişkın, R.; Çakır, E. A Data-Driven Bayesian Network Model for Oil Spill Occurrence Prediction Using Tankship Accidents. *J. Clean. Prod.* **2022**, *370*, 133478. [CrossRef]
50. Dąbrowska, E.; Torbicki, M. Forecast of hydro–meteorological changes in Southern Baltic Sea. *Water* **2024**, *16*, e1151. [CrossRef]
51. Goerlandt, F.; Kujala, P. Traffic simulation based ship collision probability modeling. *Reliab. Eng. Syst. Saf.* **2011**, *96*, 91–107. [CrossRef]
52. Akyuz, E.; Celik, M. Utilisation of cognitive map in modelling human error in marine accident analysis and prevention. *Saf. Sci.* **2014**, *70*, 19–28. [CrossRef]
53. Wróbel, K. Searching for the origins of the myth: 80% human error impact on maritime safety. *Reliab. Eng. Syst. Saf.* **2021**, *216*, e107942. [CrossRef]
54. Cheng, K.; Lu, Z. Adaptive Bayesian support vector regression model for structural reliability analysis. *Reliab. Eng. Syst. Saf.* **2021**, *206*, e107286. [CrossRef]
55. Woloszyk, K.; Goerlandt, F.; Montewka, J. A Framework to Analyse the Probability of Accidental Hull Girder Failure Considering Advanced Corrosion Degradation for Risk-Based Ship Design. *Reliab. Eng. Syst. Saf.* **2024**, *251*, 110336. [CrossRef]
56. Dondela, R.M. Analiza Niezawodności Żyrokompasu w Zmiennych Warunkach Hydro-Meteorologicznych (eng. Analysis of Gyrocompass Reliability in Variable Hydro-Meteorological Conditions). Master's Thesis, Gdynia Maritime University, Gdynia, Poland, 2021.
57. Cydejko, J.; Puchalski, J.; Rutkowski, G. *Statki i Technologie Offshore w Zarysie (eng. Ships and Offshore Technologies in Outline)*; Trademar: Gdynia, Poland, 2011.
58. Rutkowski, G. *Eksploatacja Statków Dynamicznie Pozycjonowanych (eng. Operation of Dynamically Positioned Ships)*; Trademar: Gdynia, Poland, 2013; pp. 27–29.
59. Tidewater: "Troms Capella" Brochure. Available online: https://www.tdw.com/wp-content/uploads/2016/09/Troms-Capella-2-Page-Brochure-1651.pdf (accessed on 3 January 2026).
60. Anschütz STD 22 Naval Gyro Compass System. Available online: https://www.raytheon-anschuetz.com/fileadmin/content/Downloads_Documents/Standard_22_Naval_Singapore_2019web-1.pdf (accessed on 3 March 2026).
61. Krajczyński, E. *Okrętowe Kompasy Żyroskopowe (eng. Ship's Gyroscopic Compasses)*; Wydawnictwo Morskie: Gdańsk, Poland, 1987.
62. TDC Excellence Engineering. *Service Report 11285*; TDC Excellence Engineering: Aberdeen, UK, 2020.
63. TDC Excellence Engineering. *Service Report ME E11*; TDC Excellence Engineering: Aberdeen, UK, 2019.
64. TDC Excellence Engineering. *Service Report "Troms Capella" 24.10.19*; TDC Excellence Engineering: Aberdeen, UK, 2019.
65. International Marine Contractors Association (IMCA). There—But Not Really There. DP Event DPE 03/24, 5 November 2024. Available online: https://www.imca-int.com/resources/dp/dp-incidents/dpe-03-24-there-but-not-really-there/ (accessed on 10 October 2026).
66. European Maritime Safety Agency. *Annual Overview of Marine Casualties and Incidents 2024*; EMSA: Lisbon, Portugal, 2024. Available online: https://www.emsa.europa.eu/publications/item/5352-annual-overview-of-marine-casualties-and-incidents-2024.html (accessed on 10 October 2026).
67. European Maritime Safety Agency. *Annual Overview of Marine Casualties and Incidents 2025*; EMSA: Lisbon, Portugal, 2025. Available online: https://www.emsa.europa.eu/publications/item/5562-annual-overview-of-marine-casualties-and-incidents-2025.html (accessed on 10 October 2026).
68. International Tanker Owners Pollution Federation. *Data and Statistics on Oil Spills*; ITOPF Ltd.: London, UK, 2025. Available online: http://www.itopf.org/knowledge-resources/data-statistics/ (accessed on 3 March 2026).
69. International Tanker Owners Pollution Federation. *Oil Tanker Spill Statistics 2025*; ITOPF Ltd.: London, UK, 2026. Available online: http://www.itopf.org/knowledge-resources/data-statistics/oil-tanker-spill-statistics-2025/ (accessed on 3 March 2026).

70. International Tanker Owners Pollution Federation. *ITOPF Publishes 2025 Oil Tanker Spill Statistics*; ITOPF Ltd.: London, UK, 2026. Available online: http://www.itopf.org/news/news/itopf-publishes-2025-oil-tanker-spill-statistics/ (accessed on 3 March 2026).
71. International Tanker Owners Pollution Federation. *Oil Tanker Spill Statistics 2025 (Full Report PDF)*; ITOPF Ltd.: London, UK, 2026. Available online: http://www.itopf.org/fileadmin/uploads/itopf/data/Stats/Oil_Spill_Stats_brochure_2025_lo.pdf (accessed on 5 February 2026).

**Disclaimer/Publisher's Note:** The statements, opinions and data contained in all publications are solely those of the individual author(s) and contributor(s) and not of MDPI and/or the editor(s). MDPI and/or the editor(s) disclaim responsibility for any injury to people or property resulting from any ideas, methods, instructions or products referred to in the content.